CONTINUOUS WAVE AND PULSED SOLID STATE LASER MODEL

THESIS

Matthew D. Rotondaro
Captain, USAF

AFIT/GEP/ENP/90-D-5

DEPARTMENT OF THE AIR FORCE
AIR UNIVERSITY
AIR FORCE INSTITUTE OF TECHNOLOGY

Wright-Patterson Air Force Base, Ohio

AFIT/GEP/ENP/90-D-5

CONTINUOUS WAVE AND PULSED SOLID STATE LASER MODEL

THESIS

Matthew D. Rotondaro
Captain, USAF

AFIT/GEP/ENP/90-D-5

Approved for public release; distribution unlimited.

AFIT/GEP/ENP/90-D-5

CONTINUOUS WAVE
AND
PULSED SOLID STATE LASER MODEL

THESIS

Presented to the Faculty of the School of Engineering
of the Air Force Institute of Technology
Air University
In Partial Fulfillment of the
Requirements for the Degree of
Master of Science in Engineering Physics

Matthew D. Rotondaro, B.S.
Captain, USAF

December, 1990

Preface

A laser can be described as an analog computer. For example, in the laboratory, the inputs to a laser can be measured as a voltage and current applied to the optical pump source. The laser operates on these inputs and produces an output that can be measured as an energy or power. By observing the laser's output for various input conditions, a mathematical representation of the laser's operation can be developed. The model will be written by using these observations and mathematical conclusions to represent an Nd:YAG/Glass laser on a digital computer.

Matthew D. Rotondaro

Table of Contents

List of Figures

List of Tables

AFIT/GEP/ENP/90-D-5

Abstract

A solid state laser is modeled for use on a personal computer. The model can accurately represent Nd:YAG and Nd:Glass lasers during both continuous wave and repetitively pulsed operation. The large number of input variables allow the user to make changes to the cavity, optical pump source, and the cooling system. The model calculates the energy, power, and divergence angle of the beam along with other variables. Because of its user-friendly interface, it is possible for someone with limited laser experience to obtain useful information.

CONTINUOUS WAVE
AND
PULSED SOLID STATE LASER MODEL

I. Introduction

1.1 Description of Model

The objective of this thesis is to model a solid state laser during both repetitively pulsed and continuous wave operation, for both stable and unstable cavity designs. There were three important considerations during the construction of the model: ensure a user-friendly operating environment, model the laser accurately, and ensure useful and easy to understand outputs.

The model is broken into three major components: laser kinetics, heat transfer, and wave propagation. Each of these components has a large number of variable parameters, giving the user a wide variety of input choices (see Appendix B).

The model's most important capability is the demonstration of transient thermal effects of a repetitively pulsed laser. For example, a high-energy pulsed laser would experience changes in output energy per pulse as a function of pulse rate due to heating of the laser rod. The model could be used to make predictions about these energy changes. In addition, the model could also examine the thermal limits of the laser rod without the need to destroy a laser rod.

The lasing material is the trivalent rare earth Neodymium, with a choice of host materials including YAG, the silicate glass ED-2, and the phosphate glass Q-88. These three host materials are well documented and are heavily used in industry, making them good choices for modeling.

The software was written using Microsoft QuickBASIC because of its effortless coding environment. Most computers have some implementation of the BASIC language making the code portable to other machines. Also, BASIC is such a well known language that the user should be able to modify the code to suit his/her personal needs.

1.2 Possible Uses

The laser model has a wide variety of possible applications, but the two most interesting in terms of Air Force applications are laser radar and blinding optical sensors.

Laser radar requires a high power, short pulse, single frequency, compact, reliable laser. The compact size and reliability conditions are both met by using a diode pumped Nd:YAG laser. The high power and short pulses can be achieved by Q-switching the laser. The laser model, with its ability to accurately represent a diode pumped, Q-switched, repetitively pulsed Nd:YAG laser, could be quite useful in the design of a laser radar.

The requirements for blinding optical sensors are very similar to the requirements for a laser radar. An optical sensor can be temporarily blinded or damaged by the application of a high power pulse. A laser used to blind an optical sensor needs a high pulse repetition rate to ensure that the sensor is disabled in the amount of time available to illuminate the target. The Nd:YAG laser is well suited to this application, but it only produces light with a wavelength around 1μm, and not all sensors are in this region. By frequency doubling the output of the Nd:YAG laser the output can be shifted to the optical band, increasing the the number of available targets to include sensors in the optical region. The tradeoffs between pulse repetition rate and energy deposited per pulse on the target can be evaluated using the laser model.

II. Background/Theory

2.1 Four Level Laser

Figure 1 shows the operation of an optically pumped four-level laser. Initially, all atoms of the laser material are in the lowest level. Excitation is provided by optical pumping which moves ions from the lowest level to a wide absorption band or set of bands labeled level three. The ions populating these upper bands quickly depopulate into the upper laser level, level two, at a rate of $\frac{1}{\tau_{32}}$, where τ_{32} is the relaxation time from level three to level two. The laser transition or stimulated emission is from level two to level one. Level one then quickly depopulates down to the ground level at a rate of $\frac{1}{\tau_{10}}$. To qualify as a four-level laser, the fluorescent lifetime of the lower laser level must be short compared with the fluorescent lifetime of the upper laser level, i.e., $\frac{1}{\tau_{10}} >> \frac{1}{\tau_{21}}$. In addition, the lower level must be far enough above the ground level to prevent it from becoming thermally populated.

Figure 2 is an energy level diagram for neodymium in YAG (5). The laser transition with the best performance at room temperature is from the R_2 line to the Y_3 line, making R_2 and Y_3 the upper and lower laser levels and ${}^4F_{\frac{3}{2}}$ and ${}^4I_{\frac{11}{2}}$ the upper and lower laser manifolds. The population of a level inside of a manifold can be described using the Boltzmann distribution:

$$f_i = \frac{g_i e^{-\frac{\epsilon_i}{kT}}}{\sum_j g_j e^{-\frac{\epsilon_j}{kT}}} \tag{1}$$

where g_i is the degeneracy of level i, ϵ_i is the energy of level i, T is the temperature, and k is the Boltzmann constant.

The Boltzmann factor can be used because "$\cdots$ It is also assumed that the crystal field levels within each manifold are in quasi-thermal equilibrium at all times and thus their populations are Boltzmann distributed." (17). For example, by ob-

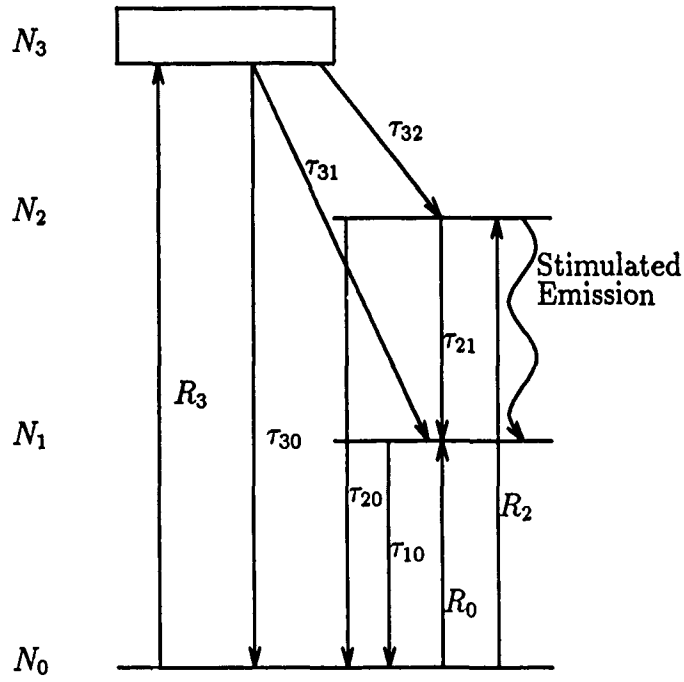

Figure 1. Simplified Energy Level Diagram of a Four-Level Laser

taining the values $g_1 = 2$, $g_2 = 2$, $\epsilon_1 = 0\ cm^{-1}$ and $\epsilon_2 = 84\ cm^{-1}$ from Appendix C, and substituting them into equation 1;

$$f_2 = \frac{2e^{-\frac{84}{0.6956T}}}{2e^0 + 2e^{-\frac{84}{0.6956T}}} \tag{2}$$

Then, at $T = 300\ K$, $f_2 = 0.40$. This means that 40 percent of the ions populating the level two manifold can be found in the R_2 level. Note, the energy of the lowest level in a manifold is always set to zero, and all subsequent levels in the manifold are measured relative to the lowest level.

2.2 Point Model

The behavior of a laser can be represented reasonably well by using a set of coupled rate equations and by assuming a spatially uniform laser medium. In the following section, the rate equations will be laid out and simplified to facilitate a numerical solution.

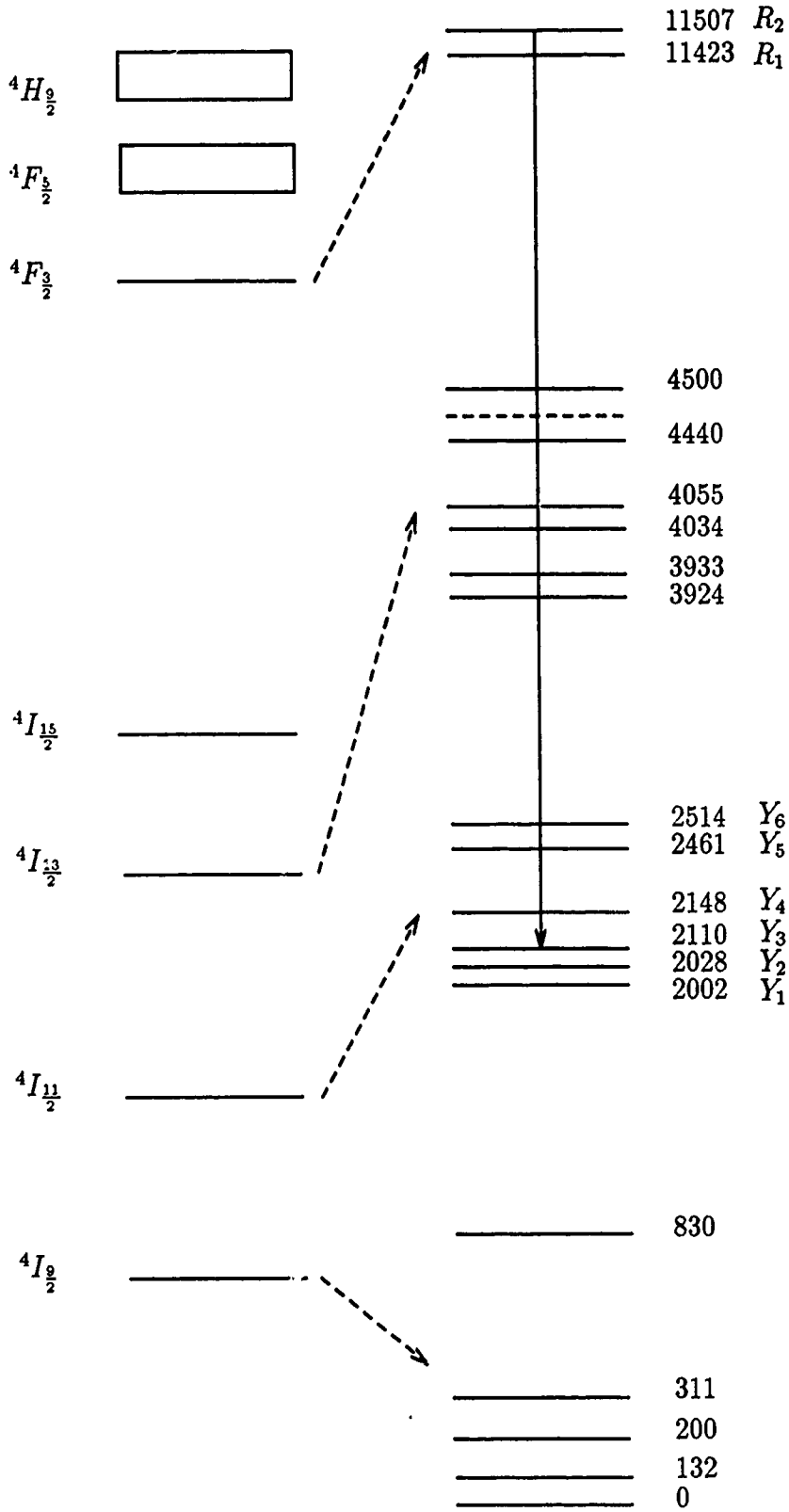

Figure 2. Energy Level Diagram for Neodymium in YAG (5)

The point model is based on the assumption that all gains and losses are evenly distributed throughout the laser cavity. More specifically, small signal gain, favorable and unfavorable losses, inversion, and photon flux are all constant with respect to position inside the cavity. This is a good assumption as long as the outcoupling is not so large as to create a substantial gradient in gain along the lasing axis. By using these assumptions and restrictions, equations 3 to 7 can be used to describe a four-level laser (17) (5) (7).

$$\frac{d\Phi}{dt} = \Phi\frac{\sigma c}{n}(N_2 - \frac{g_2}{g_1}N_1)\frac{l_r}{l_c} - \Phi\frac{\epsilon}{\tau_{rc}} + S \tag{3}$$

$$\frac{dN_3}{dt} = -\frac{N_3}{\tau_3} + R_3 \tag{4}$$

$$\frac{dN_2}{dt} = -\Phi\frac{\sigma c}{n}(N_2 - \frac{g_2}{g_1}N_1)f_2 + \frac{N_3}{\tau_{32}}f_2 - \frac{N_2}{\tau_2} + R_2 f_2 \tag{5}$$

$$\frac{dN_1}{dt} = \Phi\frac{\sigma c}{n}(N_2 - \frac{g_2}{g_1}N_1)f_1 + \frac{N_2}{\tau_{21}}\frac{f_1}{f_2} + \frac{N_3}{\tau_{31}}f_1 - \frac{N_1}{\tau_{10}} + R_1 f_1 \tag{6}$$

$$\frac{dN_0}{dt} = \frac{N_1}{\tau_{10}f_1} + \frac{N_2}{\tau_{20}f_2} + \frac{N_3}{\tau_{30}} - R_1 - R_2 - R_3 \tag{7}$$

Equation 3 describes the change in the number of photons in the cavity as a function of time. The first term on the right side of the equation is the increase due to stimulated emission. The ratio $\frac{l_r}{l_c}$ accounts for the rod being shorter than the cavity and therefore distributes the rate of stimulated emission across the whole cavity. The second term is the number of photons lost in the cavity per round trip, and the last term is the rate of spontaneous emission. Note, the spontaneous emission term is very small but can not be discarded because it is responsible for starting the lasing process.

Table 1. Definition of the Symbols in Rate Equations 3 to 7

Φ	Photons per unit volume
N_x	Number of ions in level x where x = 0,1,2,3
R_x	Number of ions excited to manifold x where x = 1,2,3
g_x	Degeneracy of level x where x = 1,2
f_x	Boltzmann factor for level x where x = 1,2
τ_x	Rate at which ions depopulate level x to all lower levels where x = 1,2,3
$\tau_{x,y}$	Rate of ion depopulation from level x to level y
τ_{rc}	Time it takes light to complete one round trip inside the cavity
l_c	Length of the cavity
l_r	Length of the rod
ϵ	Photon losses per cavity round trip
σ	Stimulated emission cross-section
n	Index of refraction of the laser medium
S	Rate of spontaneous emission into the 0,0 transverse mode
c	Speed of light in a vacuum

Equation 4 describes the change in the number of ions excited to the level three manifold as a function of time. The first term on the right side of the equation is the loss from the level three manifold to all lower levels, through phonon relaxation. The second term is the increase due to absorption of energy by the ions from the optical pump source.

Equation 5 describes the change in the number of ions populating the upper laser level as a function of time. The first term on the right side of the equation is the loss from level two due to stimulated emission. The second term is the increase to level two from the pump bands (level three) through phonon relaxation. The third term is the loss from level two to all lower levels through spontaneous emission and through phonon relaxation. The last term is the increase due to the optical pump source. The Boltzmann factor f_2 is necessary because a change of one ion in the level two manifold only changes the upper laser level by the amount f_2.

Equation 6 describes the change in the number of ions occupying the lower

laser level as a function of time. The first term on the right side of the equation is the increase in the lower level due to stimulated emission. The second and third terms are the increases to level one from levels two and three through spontaneous emission and phonon relaxation. The Boltzmann factor f_2 is in the denominator of the second term to account for the increase from manifold two, not just the increase from level two. The fourth term is the loss from level one to the ground state due to phonon relaxation and the last term is the increase due to the optical pump source. The Boltzmann factor f_1 is necessary because a change of one ion in the level one manifold only changes the level by the amount f_1.

Equation 7 describes the change in the number of ions populating the ground level as a function of time. The first three terms are the ions that eventually make it back down to the ground level after being excited to the upper manifolds. The last three terms are the losses to the ground state level due to optical pumping of the upper manifolds. The Boltzmann factors f_1 and f_2 are included in the first and second terms to account for the increase to the ground level from manifolds 1 and 2, not just from levels 1 and 2.

These five rate equations are really more than is needed to explain what is going on during the laser operation. The first simplification is the elimination of equation 7. For Nd:YAG and Nd:Glass lasers only a small fraction of the total number of ions in the ground state are ever moved to the higher levels–usually on the order of only 1 percent. This implies that, during the entire lasing process, the total number of ions in the ground state is approximately equal to the total number of ions. Because the number of ions in the ground state does not change significantly then the absorption of pump energy from the ground state ions remains constant throughout the lasing process and the number of ions in the ground state does not need to be tracked throughout the lasing process.

The next simplification is a bit more rigorous. Equation 4 can be neglected when $\tau_{32} \leq \frac{Pump\ Duration}{100}$. Equation 4 has a solution of the form

$$N_3 = R_3\tau_3(1 - \exp(\frac{-t}{\tau_3})) \tag{8}$$

where

$$\frac{1}{\tau_3} = \frac{1}{\tau_{30}} + \frac{1}{\tau_{31}} + \frac{1}{\tau_{32}} \tag{9}$$

and

$$\tau_{32} \ll \tau_{31}, \tau_{30} \tag{10}$$

Therefore

$$N_3 \approx R_3\tau_{32}(1 - \exp(\frac{-t}{\tau_{32}})) \tag{11}$$

This equation shows that when t is greater than 1 μs and τ_{32} is 100 ns or smaller then

$$N_3 \approx R_3\tau_{32} \tag{12}$$

where t is the amount of time the flash lamp is on and is typically greater than 1 μs.

Equation 12 can be substituted directly into equation 5 to yield

$$\frac{dN_2}{dt} = -\Phi\frac{\sigma c}{n}(N_2 - \frac{g_2}{g_1}N_1)f_2 + R_3f_2 - \frac{N_2}{\tau_2} + R_2f_2 \tag{13}$$

and by letting $R_2' = R_2 + R_3$ then

$$\frac{dN_2}{dt} = -\Phi\frac{\sigma c}{n}(N_2 - \frac{g_2}{g_1}N_1)f_2 - \frac{N_2}{\tau_2} + R_2'f_2 \tag{14}$$

This means that if τ_{32} is 100ns or smaller, then equation 4 can be eliminated and the manifold pump rate R_3 can be directly added to the manifold two pump rate.

The pump rates are, in general, very difficult to calculate. They require the modeling of both the optical pump source and the absorption of the lasing material. Such an undertaking would be a considerable amount of work and would be outside the scope of this project. Therefore, the following approximation is used to calculate the pump rate R_2'.

$$R_2' = \frac{Electrical\ power\ into\ the\ lamp\ x\ The\ fraction\ for\ lasing}{h\ x\ Laser\ frequency\ x\ Volume\ of\ the\ rod} \tag{15}$$

where *Electrical power into the lamp* and *The fraction for lasing* are user inputs (see Appendix B) and h is Planck's constant. This is a good approximation for the Nd ion lasers because, as stated earlier, the absorption cross-section can be treated as a constant. Therefore, the pump rate is constant and determined only by a fraction of the flash lamp input electrical power.

The model is designed to accurately represent the output of a pulsed laser. A subset of the pulsed laser is the Q-switched laser. The Q-switch is a device placed inside the laser cavity and is generally used to generate high pulse powers. The Q-switch prevents the laser from lasing by spoiling the quality of the cavity. This is done so that the population inversion can build past the minimum inversion required to lase; the critical inversion N_{Crit}. Finally, by the time the Q-switch is opened and lasing is allowed to take place, the inversion has increased well above the critical inversion. This large inversion produces a large gain in the cavity causing the number of photons to build very rapidly. The rapid buildup in photons extracts the energy from the inversion very quickly producing the desired high power output pulse.

While the quality of the cavity is spoiled by the Q-switch, the number of photons in the cavity is approximately equal to zero. Therefore $\Phi = 0$ and equation 14 can be written as

$$\frac{dN_2}{dt} = -\frac{N_2}{\tau_2} + R_2' f_2 \tag{16}$$

which has the following solutions for the specified domains

$$N_2 = R_2' \tau_2 f_2 (1 - \exp(\frac{-t}{\tau_2})) \quad 0 \leq t \leq t_{Q-switch} \leq T \tag{17}$$

and

$$N_2 = N_2(T) \exp(\frac{T-t}{\tau_2}) \quad T \leq t \leq t_{Q-switch} \tag{18}$$

where T is the time at which the flash lamp was turned off, and $t_{Q-switch}$ is the time that Q-switching occurred.

Even after these simplifications, equations 3 to 7 are still a set of nonlinear coupled differential equations which require numerical techniques to solve. In order to apply numerical techniques, it is advisable to first normalize the equations.

A quantity well suited to the normalization of the rate equations is the critical inversion. The critical inversion is the minimum inversion necessary to achieve lasing and is defined during steady state operation. Steady state means that the net change in the number of photons per unit time in the cavity is equal to zero:

$$\frac{d\Phi}{dt} = 0 \tag{19}$$

Equation 3 may now be written as

$$\frac{\epsilon}{\tau_{rc}} = \frac{\sigma c}{n}(N_2 - \frac{g_2}{g_1} N_1) \frac{l_r}{l_c} + S \tag{20}$$

The spontaneous emission rate S is given by (7)

$$S = \frac{N_2}{\tau_{21}} \frac{c^3}{8\pi\nu^2 \Delta\nu V_{Cavity}} \tag{21}$$

where

ν = The laser frequency,

$\Delta\nu$ = FWHM of the lineshape for atomic response,

V_{Cavity} = volume of the laser cavity.

Noting that S is very small and may be neglected allows the critical inversion to be defined as

$$N_{Crit} \equiv (N_2 - \frac{g_2}{g_1} N_1) = \frac{\epsilon n}{\tau_{rc} \sigma c} \frac{l_c}{l_r} \tag{22}$$

Another parameter useful for normalizing the rate equations is the cavity lifetime (7).

$$\tau_{cav} \equiv \frac{Cavity\ round\ trip\ time}{Fractional\ round\ trip\ loss} \tag{23}$$

The cavity life time for a stable cavity is given by (7)

$$\tau_{cav} = \frac{2}{c}[n l_r + (l_c - l_r)] \left[\frac{1}{\ln(\frac{1}{R_1 R_2}) + 2\alpha l_r + \ln(\frac{1}{Q})} \right] \tag{24}$$

Table 2. Definition of Terms for the Stable Cavity Lifetime

R_1	Reflectivity of mirror one = 1 - fractional outcoupling
R_2	Reflectivity of mirror two = 1 - absorption losses
$\ln(\frac{1}{R_1 R_2})$	Losses at the mirrors
$2\alpha l_r$	Losses due to the rod
Q	Transmission of the Q-switch
$\ln(\frac{1}{Q})$	Losses due to the addition of a Q-switch into the cavity

The cavity life time for an unstable cavity is given by

$$\tau_{cav} = \frac{2}{c}[nl_r + (l_c - l_r)]\left[\frac{1}{\ln(\frac{1}{R_1 R_2 \Gamma}) + 2\alpha l_r + \ln(\frac{1}{Q})}\right] \tag{25}$$

Table 3. Definition of Terms for the Unstable Cavity Lifetime

R_1	Reflectivity of mirror one = 1 - absorption losses
R_2	Reflectivity of mirror two = 1 - absorption losses
$\ln(\frac{1}{R_1 R_2 \Gamma})$	Losses at the mirrors and unstable cavity outcoupling
$2\alpha l_r$	Losses due to the rod
Q	Transmission of the Q-switch
Γ	1 - Unstable cavity outcoupling
$\ln(\frac{1}{Q})$	Losses due to the addition of a Q-switch into the cavity

$$\epsilon = \frac{\tau_{rc}}{\tau_{cav}} \tag{26}$$

$$N_{Crit} = \frac{n}{\sigma c \tau_{cav}} \frac{l_c}{l_r} \tag{27}$$

Now, normalization can proceed by using the following expressions:

$$\phi = \frac{\Phi}{N_{Crit}} \tag{28}$$

$$n_x = \frac{N_x}{N_{Crit}} \tag{29}$$

$$t_{x,y} = \frac{\tau_{x,y}}{\tau_{cav}} \tag{30}$$

$$t_x = \frac{\tau_x}{\tau_{cav}} \tag{31}$$

$$r_x = R_x \frac{\tau_{cav}}{N_{Crit}} \tag{32}$$

$$s = S\frac{\tau_{cav}}{N_{Crit}} \tag{33}$$

Finally writing the normalized equations as

$$\frac{d\phi}{dt} = \phi(n_2 - \frac{g_2}{g_1}n_1) - \phi + s \tag{34}$$

$$\frac{dn_3}{dt} = -\frac{n_3}{t_3} + r_3 \tag{35}$$

$$\frac{dn_2}{dt} = -\phi(n_2 - \frac{g_2}{g_1}n_1)f_2\frac{l_c}{l_r} + \frac{n_3}{t_{32}}f_2 - \frac{n_2}{t_2} + r_2 f_2 \tag{36}$$

$$\frac{dn_1}{dt} = \phi(n_2 - \frac{g_2}{g_1}n_1)f_1\frac{l_c}{l_r} + \frac{n_2}{t_{21}}\frac{f_1}{f_2} + \frac{n_3}{t_{31}}f_1 - \frac{n_1}{t_{10}} + r_1 f_1 \tag{37}$$

and for the case when τ_{32} is of the order of 100ns or smaller, then

$$\frac{d\phi}{dt} = \phi(n_2 - \frac{g_2}{g_1}n_1) - \phi + s \tag{38}$$

$$\frac{dn_2}{dt} = -\phi(n_2 - \frac{g_2}{g_1}n_1)f_2\frac{l_c}{l_r} - \frac{n_2}{t_2} + r_2' f_2 \tag{39}$$

$$\frac{dn_1}{dt} = \phi(n_2 - \frac{g_2}{g_1}n_1)f_1\frac{l_c}{l_r} + \frac{n_2}{t_{21}}\frac{f_1}{f_2} + \frac{r_3 t_{32}}{t_{31}}f_1 - \frac{n_1}{t_{10}} + r_1 f_1 \tag{40}$$

The last thing that needs to be determined before integration can proceed is the stimulated emission cross-section σ. The stimulated emission cross-section is given by (5) as

$$\sigma = A_{21}\frac{\lambda^2}{8\pi n^2}g(\nu) \tag{41}$$

where

A_{21} = The Einstein A-coefficient

λ = The laser wavelength

n = The index of refraction in the rod

$g(\nu)$ = The atomic line shape

Thermal broadening is the mechanism responsible for the linewidth of the Nd:YAG laser. "Thermal broadening is brought about by the effect of thermal lattice vibrations on the atomic transition. The thermal vibrations of the lattice surrounding the active ions modulate the resonance frequency of each atom at a very high frequency. This frequency modulation represents a coupling mechanism between the atoms, therefore a homogeneous linewidth is obtained."(7) The homogeneous linewidth leads to a Lorentzian line shape for atomic response, such that

$$g(\nu) = \left(\frac{\Delta\nu}{2\pi}\right)\left[(\nu - \nu_0)^2 + (\frac{\Delta\nu}{2})^2\right]^{-1} \tag{42}$$

The laser model assumes lasing only at the central peak ν_0 and therefore the line shape can be reduced to

$$g(\nu) = \frac{2}{\pi\Delta\nu} \tag{43}$$

An inhomogeneously broadened line shape occurs in the fluorescence of a neodymium doped glass. "There are variations from rare earth site to rare earth site in the relative atomic positions occupied by the surrounding lattice ions. This gives rise to a random distribution of static crystalline fields acting on the rare earth ions. Since the line shifts corresponding to such crystal-field variations are larger, generally speaking, than the width contributed by other factors associated with the transition, an inhomogeneous line results."(7) The inhomogeneous line can be represented by a Gaussian frequency distribution given by

$$g(\nu) = \frac{2}{\Delta\nu}\left(\frac{\ln 2}{\pi}\right)^{\frac{1}{2}} \exp\left[-\left(\frac{\nu-\nu_0}{\frac{\Delta\nu}{2}}\right)^2 \ln 2\right] \tag{44}$$

Again, the laser model assumes lasing only at the central peak ν_0 and therefore the line shape can be reduced to

$$g(\nu) = \frac{2}{\Delta\nu}\left(\frac{\ln 2}{\pi}\right)^{\frac{1}{2}} \tag{45}$$

Now equations 38 to 40 can be solved by using a Runga-Kutta or an Adams Predictor-Corrector method of integration (see Appendix A). The integration is needed to determine the number of photons in the cavity at any given time. Once the number of photons in the cavity is known, then the number of photons in the beam can be determined by first rewriting τ_{cav} in equation 3 in terms of favorable and unfavorable losses.

$$\frac{d\Phi}{dt} = \Phi\frac{\sigma c}{n}(N_2 - \frac{g_2}{g_1}N_1)\frac{l_r}{l_c} - \frac{\Phi}{\tau_{fav}} - \frac{\Phi}{\tau_{unfav}} + S \tag{46}$$

Favorable losses are the losses that go into the laser output, and unfavorable losses include losses in the rod, Q-switch, and the back mirror.

$$\frac{1}{\tau_{cav}} = \frac{1}{\tau_{fav}} + \frac{1}{\tau_{unfav}} \tag{47}$$

Separating out the favorable losses from equation 46,

$$\frac{d\Phi_{beam}}{dt} = \frac{\Phi}{\tau_{cav}} \tag{48}$$

This is the number of photons in the beam per unit volume per unit time, where τ_{fav} for a stable cavity is given by

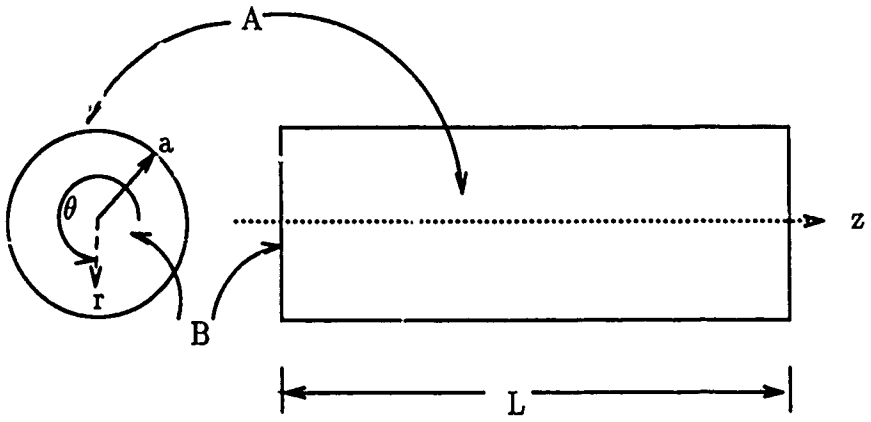

Figure 3. Geometry of the Laser Rod

$$\tau_{fav} = \frac{2}{c}[nl_r + (l_c - l_r)]\left[\frac{1}{\ln(\frac{1}{R_1})}\right] \tag{49}$$

and τ_{fav} for an unstable cavity is given by

$$\tau_{fav} = \frac{2}{c}[nl_r + (l_c - l_r)]\left[\frac{1}{\ln(\frac{1}{\Gamma})}\right] \tag{50}$$

2.3 Nodal Network Heat Transfer

An inherent effect of shining a light on the laser rod to pump the laser inversion is the heating of the rod. This heating is responsible for thermal lensing, birefringence, stress fractures, and in extreme cases, melting the rod. Therefore, a description of the temperature distribution in the rod is necessary to accurately describe the laser. In this section the temperature distribution in the rod will be found by solving equation 51 which describes the heat flow in a flash lamp pumped, fluid cooled rod (2).

$$c_p(T)\rho(T)\frac{dT}{dt} = \nabla \cdot (k(T)\nabla T) + q^*(r,\theta,z) \tag{51}$$

The temperature $T = T(r,\theta,z,t)$ and is subject to the following boundary conditions:
$T(0,\theta,z,t) < \infty$

$T(r,0,z,t) = T(0,2\pi,z,t)$

$\frac{dT(r,\theta,z,t)}{dr})_{r=R} = \frac{h_{film}}{k}(T(R,\theta,z,t) - T_{film})$

$\frac{dT(r,\theta,z,t)}{dr})_{z=0} = \frac{h_{air}}{k}(T(r,\theta,0,t) - T_{air})$

$\frac{dT(r,\theta,z,t)}{dr})_{z=L} = \frac{h_{air}}{k}(T(r,\theta,L,t) - T_{air})$

$T(r,\theta,z,0) = T_{fluid}$

Table 4. Definition of Terms for the Heat Equation

T	Temperature distribution in the rod
c_p	Heat capacity of the rod
ρ	Density of the rod
k	Thermal conductance of the rod
q^*	Heat energy entering the rod per unit volume
A	Surface area normal to $\hat{r}$. See figure 3
B	Surface area normal to $\hat{z}$. See figure 3
T_{film}	Temperature of the fluid film surrounding area A
T_{air}	Temperature of the air surrounding area B

Equation 51 is very difficult to solve, and is more general than is required to do an accurate job of describing the heat flow in the laser rod. The equation can be simplified by eliminating the θ and z dependence. This is accomplished by using the following three assumptions: $q^* = Constant$, the heat flow at the ends of the rod is small, and the fluid flow on surface A is fast enough to ensure that the fluid temperature does not change significantly as it travels the length of the laser rod. Using these assumptions, equation 51 can be reduced to

$$c_p(T)\rho(T)\frac{dT}{dt} = \nabla \cdot (k(T)\nabla T) + q^* \tag{52}$$

The temperature $T = T(r,t)$ and is subject to the following boundary conditions:

$T(0,t) < \infty$

$\frac{dT(r,t)}{dr})_{r=R} = \frac{h}{k}(T(R,t) - T_{film})$

$T(r,0) = T_{fluid}$

This can be further simplified by assuming that c_p, ρ and k are constants, yielding

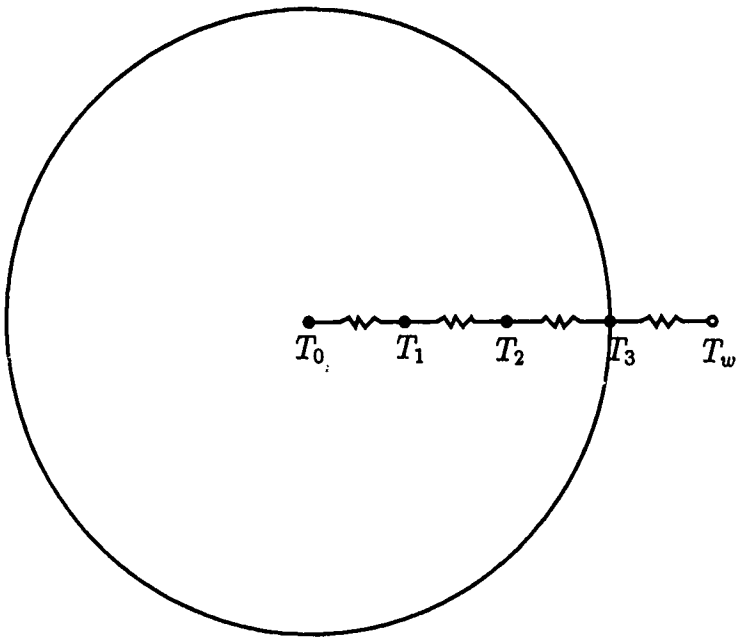

Figure 4. One Dimensional Heat Transfer Nodal Network

$$\frac{dT}{dt} = \frac{k}{c_p \rho} \nabla^2 T + \frac{q^*}{c_p \rho} \tag{53}$$

The temperature $T = T(r,t)$ is subject to the following boundary conditions:

$T(0,t) < \infty$

$\frac{dT(r,t)}{dr})_{r=R} = \frac{h}{k}(T(R,t) - T_{film})$

$T(r,0) = T_{fluid}$

The heat q^* is given by

$$q^* = \frac{Flash\ Lamp\ Wattage\ x\ Power\ Fraction\ Heat}{Laser\ Rod\ Volume} \tag{54}$$

where *Flash Lamp Wattage*, *Power Fraction Heat*, and *Laser Rod Volume* are all user inputs (see Appendix B).

An approximate solution may be had by using a finite difference approximation (see Figure 4) (2). The solution to equation 53 can be written as

$$T_i' = T_i + \delta t \left[\sum_j \frac{T_i - T_j}{\mathcal{R}_{ij} C_i} + \frac{q_i}{C_i} \right] \tag{55}$$

where the thermal resistance between nodes i and j for conduction inside the rod is

$$\mathcal{R}_{ij} = \frac{\delta r}{k A_{ij}} \tag{56}$$

the thermal resistance between nodes i and j for convection at the rods surface is

$$\mathcal{R}_{ij} = \frac{1}{h A_{ij}} \tag{57}$$

and the thermal capaciy for node i is given by

$$C_i = V_i \rho c_p \tag{58}$$

Table 5. Definition of Terms for the Finite Difference Solution to the Heat Equation

T_i	Temperature at node i
T_i'	Temperature at node i at a time $t + \delta t$
q_i	Heat input at node i
δr	Distance between nodes
δt	Time step
h	Heat transfer coefficient for the cooling fluid
A_{ij}	Surface area evaluated half-way between node i and j
C_i	Thermal capacity for node i
V_i	Volume of node i
ρ	Density of the rod material
c_p	Heat capacity of the rod material

"These equations just given express the temperature at a given node in terms of a discrete spatial step δr and discrete time step δt. The important point is that the continuous solution of the original differential equation is replaced by a numerical

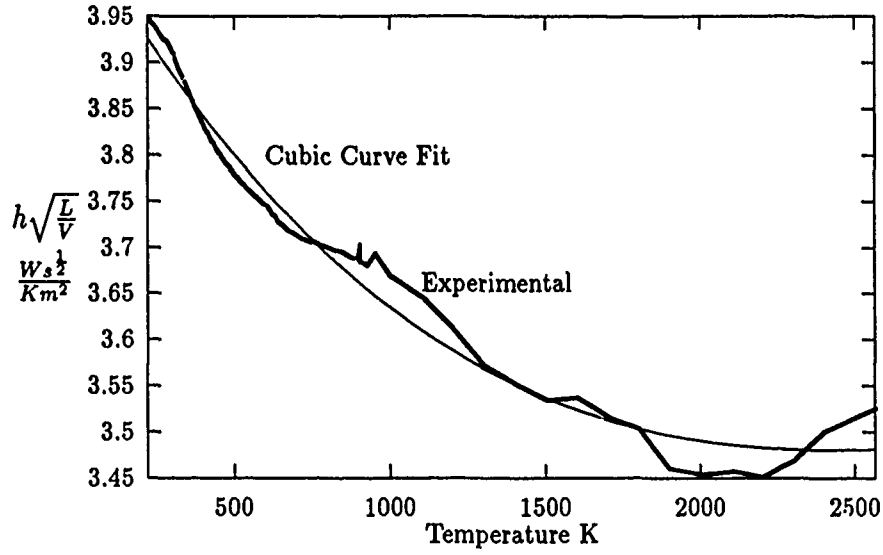

Figure 5. Experimental vs Cubic Curve Fit for Air

solution of these difference equations at particular points in space and at particular intervals of time."(2)

The solution is only stable if δt is selected such that (2)

$$\delta t \leq \frac{1}{\frac{1}{\sum_j \mathcal{R}_{ij} C_i}} \tag{59}$$

The smallest δt for all nodes is the one necessary to insure stability of the solution (2). "The implication of equation 59 is that the choice of the time step δt is intimately connected with the choice of the spatial increment, δr, which is involved in the resistance $\mathcal{R}_{ij}$. As smaller spatial increments are chosen to reduce the associated truncation error, smaller time increments must also be used in order to satisfy equation 59. Thus, increased accuracy in the spatial network is obtained at the cost of smaller time increments"(2).

By using a one-dimensional nodal network (see Figure 4), the radial temperature distribution in the rod can be found. Initially, the temperature at all of the nodes is equal to the temperature of the water T_w surrounding the laser rod. When

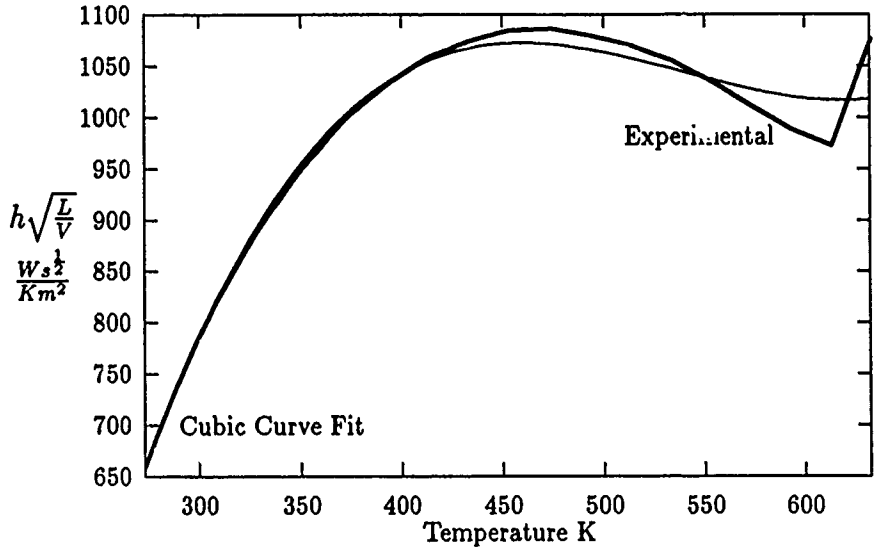

Figure 6. Experimental vs Cubic Curve Fit for Water

the rod is heated through flash lamp pumping, it is assumed that the rod heats up uniformly. As the temperature of the laser rod increases a temperature gradient between the rod and the water develops and heat begins to flow out of the rod creating a parabolic temperature distribution in the rod.

The nodal network solution allows for generalization to the more complex cases where the heat capacity and thermal conductivity are not constants. Another advantage to reducing the more general case with the variable conductivity and heat capacity is that the steady state solution is easily evaluated and can be used to validate the numerical solution before generalizing to the more complex case.

At the surface of the rod the thermal resistance is given by equation 57. This resistance is dependent on the heat transfer coefficient h. The heat transfer coefficient is a function of temperature and velocity. Figures 5 and 6 are plots of $h\sqrt{\frac{L}{V}}$ verses temperature for dry air and water (2)(6). The second curve in each figure is a third degree polynomial curve fit.

$$h\sqrt{\frac{L}{V}} = 4.04562 - 5.82881x10^{-4}T_{film} + 1.92359x10^{-7}T_{film}^2 - 1.98457x10^{-11}T_{film}^3 \quad (60)$$

for air, and

$$h\sqrt{\frac{L}{V}} = -3058.2 + 23.891T_{film} - .045303T_{film}^2 + 2.80149x10^{-5}T_{film}^3 \qquad (61)$$

for water. L is the length of the laser rod, and V is the velocity of the coolant flowing over the rod.

When a fluid of one temperature flows over a rod at a different temperature, a thermal boundary layer develops. Good results are obtained when the fluid properties are evaluated at the film temperature T_{film} given by the following approximation(6):

$$T_{film} = \frac{T_{fluid} + T_{wall}}{2} \qquad (62)$$

The finite difference solution is general enough to describe the temperature distribution in the rod at any time t. The problem with the finite difference solution is that as $t \rightarrow \infty$, the computational time also goes to infinity. This condition is encountered by a continuous wave laser. The resolution to this problem can be found by recognizing that equation 53 has an analytic solution in the steady state limit. See Chapter 3 for details.

The problem with the analytic solution is that it depends on the heat transfer coefficient which is a function of temperature. Because of this dependence, the analytic steady state solution is really a transcendental equation. Using the steady state solution from Chapter 3,

$$T(R) = \frac{T_{fluid} + T(R)}{2} + \frac{q^*}{4k}\left[\frac{2kR}{h(T(R))}\right] \qquad (63)$$

By solving this transcendental equation for T(R), and by using the steady state solution in Chapter 3, the steady state temperature distribution in the rod can be found.

2.4 Transient Thermal Effects

As the rod changes temperature the index of refraction also changes. This change in index can be described by the following expression:

$$n_o = n - [300 - T(0)]\frac{dn}{dT} \tag{64}$$

where n_o is the index of refraction at the center of the rod, n is the index of refraction of the material at $300°K$, T(0) is the temperature at the center of the rod, and $\frac{dn}{dT}$ is the change in index of refraction with respect to temperature. The index of refraction as a function of radius is given by

$$n(r) = n_o + [T(r) - T(0)]\frac{dn}{dT} \tag{65}$$

This change in index accounts for the thermal lensing in the rod. Note, for example, that if $\frac{dn}{dt}$ is positive, and the rod is hotter at the center than on the walls, then the rod will act like a positive lens.

2.5 Beam Quality

The model can be used to analyze a laser with a stable or an unstable cavity. Knowing the cavity design is very important because the techniques for determining information about the beam are very different for the two cases. In this section the method of determining the stability of a cavity will be derived. This will be followed by a discussion of the techniques used for determining spot size, mode volume, and divergence angle for a stable cavity. The section will then conclude with a discussion of the techniques used to determine the outcoupling, spot size, and divergence angle for an unstable cavity.

2.5.1 **Stability** A cavity is considered stable if a ray inside the cavity can go through an infinite number of round trips and still remain inside the cavity. If

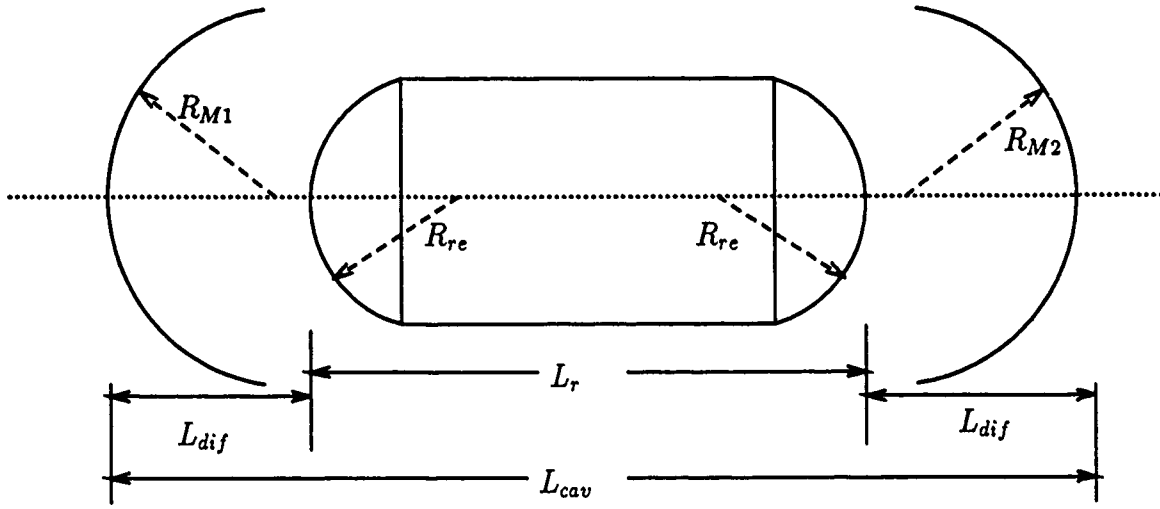

Figure 7. The Cavity Design Used by the Laser Model

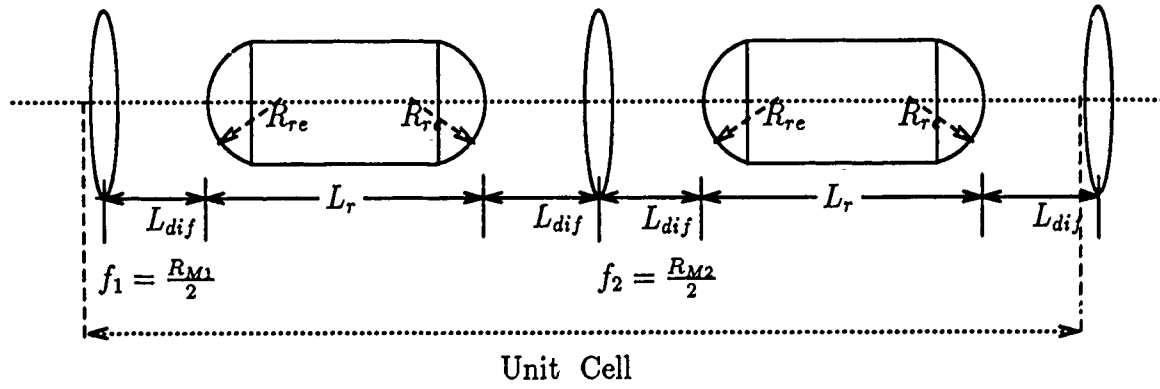

Figure 8. Equivalent Cavity Lens Wave Guide

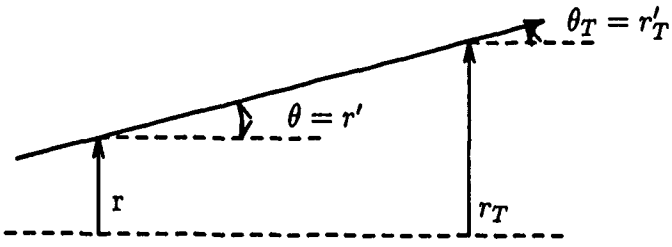

Figure 9. A Ray Traversing a Length of Space

the rays were able to "walk" out of the cavity then the cavity would be considered unstable. Stability can be found by using transformation matrices that transform an input ray at position z to the position z' (see Figure 9). The transformation matrices are constructed based on a paraxial approximation; $\tan(\theta) \approx \sin(\theta) \approx \theta = r'$. Figure 7 depicts the cavity design used by the laser model. Figure 8 is the equivalent lens wave guide. The following matrices describe the round trip propagation of a ray through the cavity (12) (9) (8) (5).

$$\begin{bmatrix} r_T \\ r'_T \end{bmatrix} = \begin{pmatrix} 1 & L_{dif} \\ 0 & 1 \end{pmatrix} \begin{pmatrix} 1 & 0 \\ \frac{1-n}{R_{re}} & n \end{pmatrix} \begin{pmatrix} \cos(b) & \frac{L_{rod}}{n_0 b}\sin(b) \\ -\frac{n_0 b}{L_{rod}}\sin(b) & \cos(b) \end{pmatrix} \tag{66}$$
$$\begin{pmatrix} 1 & 0 \\ -\frac{n-1}{nR_{re}} & \frac{1}{n} \end{pmatrix} \begin{pmatrix} 1 & L_{dif} \\ 0 & 1 \end{pmatrix} \begin{pmatrix} 1 & 0 \\ -\frac{2}{R_{M2}} & 1 \end{pmatrix} \begin{pmatrix} 1 & L_{dif} \\ 0 & 1 \end{pmatrix}$$
$$\begin{pmatrix} 1 & 0 \\ \frac{1-n}{R_{re}} & n \end{pmatrix} \begin{pmatrix} \cos(b) & \frac{L_{rod}}{n_0 b}\sin(b) \\ -\frac{n_0 b}{L_{rod}}\sin(b) & \cos(b) \end{pmatrix} \begin{pmatrix} 1 & 0 \\ -\frac{n-1}{nR_{re}} & \frac{1}{n} \end{pmatrix}$$
$$\begin{pmatrix} 1 & L_{dif} \\ 0 & 1 \end{pmatrix} \begin{pmatrix} 1 & 0 \\ -\frac{2}{R_{M1}} & 1 \end{pmatrix} \begin{bmatrix} r \\ r' \end{bmatrix}$$

where

n = Index of refraction averaged across the radial direction.

n_0 = Index of refraction at the center of the rod.

n_R = Index of refraction at the surface of the rod.

$$n_R = n_0 - \frac{\eta R^2}{2} \tag{67}$$

$$n = \frac{2n_0 + n_R}{3} \tag{68}$$

$$\eta = \frac{2(n_0 - n_R)}{R^2} \tag{69}$$

$$b = L_{rod}\sqrt{\frac{\eta}{n_0}} \tag{70}$$

and where

$$\begin{pmatrix} \cos(b) & \frac{L_{rod}}{n_0 b}\sin(b) \\ \frac{n_0 b}{L_{rod}}\sin(b) & \cos(b) \end{pmatrix} \tag{71}$$

is the transformation matrix for a laser rod acting like a positive lens.

When $n_R > n_0$, the rod acts like a diverging lens, and b becomes imaginary. By letting b = iB where $B = L_{rod}\sqrt{-\frac{\eta}{n_0}}$ and using some very well known trigonometric identities $[Cos(i\theta) = Cosh(\theta)]$ and $[Sin(i\theta) = iSinh(\theta)]$ the transformation matrix for a laser rod acting like a diverging lens can be written as

$$\begin{pmatrix} \cosh(B) & \frac{L_{rod}}{n_0 B}\sinh(B) \\ \frac{n_0 B}{L_{rod}}\sinh(B) & \cosh(B) \end{pmatrix} \tag{72}$$

By multiplying the matrices in equation 67 together from right to left, equation 67 can be written as

$$\begin{bmatrix} r_T \\ r'_T \end{bmatrix} = \begin{pmatrix} A & B \\ C & D \end{pmatrix} \begin{bmatrix} r \\ r' \end{bmatrix} \tag{73}$$

Completing the multiplication, the following recurrence relations can be written:

$$r_{T+1} = Ar_T + Br'_T \Rightarrow r'_T = \frac{1}{B}(r_{T+1} - Ar_T) \tag{74}$$

$$r'_{T+1} = Cr_T + Dr'_T \tag{75}$$

$$r'_{T+1} = \frac{1}{B}(r_{T+2} - Ar_{T+1}) = Cr_T + Dr'_T \tag{76}$$

$$\frac{1}{B}(r_{T+2} - Ar_{T+1}) = Cr_T + \frac{D}{B}(r_{T+1} - Ar_T) \tag{77}$$

$$r_{T+2} - 2\frac{A+D}{2}r_{T+1} + (AD - BC)r_T = 0 \tag{78}$$

This second-order difference equation describes the rays that pass through any cavity represented by an ABCD matrix. The solution will be found by assuming a solution of the form $r_T = r_o e^{i\theta T}$. Substituting this solution into equation 78 yields

$$r_o e^{i\theta T}\left[e^{i2\theta} - 2\frac{A+D}{2}e^{i\theta} + (AD - BC)\right] = 0 \tag{79}$$

In order for there to be a non-trivial solution, the expression inside of the brackets must be equal to zero. Therefore, $e^{i\theta}$ can be found by using the quadratic equation:

$$e^{i\theta} = \frac{A+D}{2} \pm i\left[AD - BC - \left(\frac{A+D}{2}\right)^2\right]^{\frac{1}{2}} \tag{80}$$

In order for the solution to be oscillatory,

$$AD - BC - \left(\frac{A+D}{2}\right)^2 > 0 \tag{81}$$

and therefore, to ensure stability inside the cavity:

$$|A + D| < 2\sqrt{AD - BC} \tag{82}$$

2.5.2 **Stable Cavity** Once the stability of the cavity has been determined, the spot size of the beam everywhere along the lasing axis must be found. This will allow the determination of the mode volume, and the divergence angle of the beam. In order to find the spot size for a stable cavity it will be necessary to introduce the complex beam parameter q (5):

$$\frac{1}{q} = \frac{1}{R} - i\frac{\lambda}{\pi n w^2} \tag{83}$$

where

R = radius of curvature of the wave front

w = radius of the spot defined, as the point where the intensity falls off to $\frac{1}{e^2}$ of the peak intensity for the 0,0 transverse mode.

If the radius R and the spot size w are known at some position inside the cavity, then it is possible to find the complex beam parameter at any other point inside the cavity by using the expression

$$\frac{1}{q_2} = \frac{C + \frac{D}{q_1}}{A + \frac{B}{q_1}} \tag{84}$$

where the matrix

$$\begin{pmatrix} A & B \\ C & D \end{pmatrix} \tag{85}$$

is a transformation matrix from the point of known q to the point where q needs to be determined. At a mirror of a stable cavity, the radius of curvature of the wavefront is the same as the radius of curvature of the mirror. Also, for a round trip in a stable cavity, $q_1 = q_2$. Therefore defining

$$x \equiv \frac{1}{R} \tag{86}$$

and

$$y \equiv \frac{\lambda}{\pi n w^2} \tag{87}$$

equation 84 can be written as

$$x_2 - iy_2 = \frac{C + D(x_1 - iy_1)}{A + B(x_1 - iy_1)} \tag{88}$$

Separating into real and imaginary parts:

$$x_2 = \frac{AC + (AD + BC)x_1 + BD(x_1^2 + y_1^2)}{A^2 + 2ABx_1 + B^2(x_1^2 + y_1^2)} \tag{89}$$

$$y_2 = \frac{y_1(AD - BC)}{A^2 + 2ABx_1 + B^2(x_1^2 + y_1^2)} \tag{90}$$

at a mirror where $x_1 = x_2 = x$ and $y_1 = y_2 = y$, then

$$y = \left[\frac{AD - BC - A^2 - 2ABx}{B^2} - x^2\right]^{\frac{1}{2}} \tag{91}$$

Now that q is known at a mirror, then it can be propagated through the cavity to obtain the spot size throughout the cavity. If the spot is propagated through the rod using a small step size, δz, then the spot size everywhere in the rod can be determined. The mode volume can be calculated by

$$V_{Mode} = \delta z \sum_{i=1}^{N} \pi w_i^2 \tag{92}$$

where $\delta z = \frac{RodLength}{N}$. The mode volume is for the (0,0) cylindrical geometry transverse mode, $V_{0,0} = V_{Mode}$. The spot size for higher order transverse modes can be found by using $W_{p,l} = C_{p,l} w_{0,0}$ (7), and therefore the higher order mode volume can be found using $V_{p,l} = C_{p,l}^2 V_{0,0}$, where $C_{p,l}$ is a constant for the mode p,l. For example, $C_{0,0} = 1$, $C_{0,1} = 1.5$, $C_{1,0} = 1.9$, and $C_{1,1} = 2.15$. The highest order mode is determined by forcing twice the higher order mode spot size to be less than the

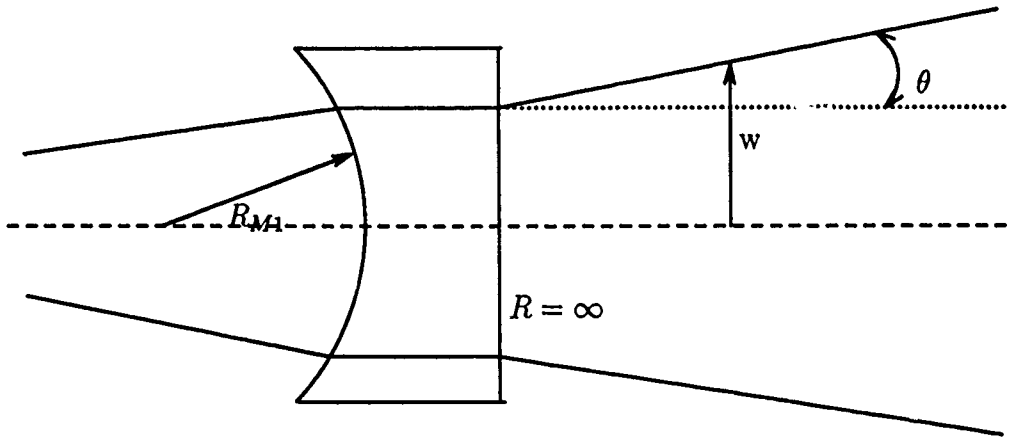

Figure 10. Stable Cavity Outcoupler

rod radius, $2W_{p,l} < R_{rod}$, at all positions inside the rod. Once the mode volume is known, then the number of ions that contribute to the lasing process is known, and an absolute value for the energy and power can be determined.

Finally, to find the spot size on target the complex beam parameter q at the outcoupler needs to be propagated through the outcoupler, and then propagated down range to the target. Therefore, the transformation matrix through the outcoupler and down range is given by

$$\begin{pmatrix} A & B \\ C & D \end{pmatrix} = \begin{pmatrix} 1 & d \\ 0 & 1 \end{pmatrix} \begin{pmatrix} 1 & 0 \\ \frac{.5}{R_{M1}} & 1 \end{pmatrix} \tag{93}$$

where d is the distance to the target. This transformation matrix was written with the assumption that the index of refraction of the outcoupler, n=1.5, the outcoupler is very thin, and the outside surface of mirror one is planar (see Figure 10). Once the spot size at the outcoupler and at the target are known, then the divergence angle can be found by

$$\theta_{Diverg} = \arctan\left(\frac{w_{target} - w_{oc}}{d}\right) \tag{94}$$

2.5.3 **Unstable Cavity** For the stable cavity, it was possible to determine the spot size everywhere along the lasing axis and thus determine mode volume and divergence angle of the beam. For the unstable cavity it is very difficult to determine the spot size inside the cavity, so a different approach will be used. This approach consists of two steps. The first step will be to find the cavity's round trip magnification, which will lead to finding the spot size at the outcoupler. The second step will be to equate the real cavity to a simplified equivalent cavity to determine the divergence angle of the beam.

The round-trip magnification can be found by returning to equation 78. This second-order difference equation describes the rays that pass through any cavity represented by an ABCD matrix. Again, the solution will be found by assuming a solution of the form $r_T = r_o F^T$. Substituting into equation 78;

$$r_o F^T \left[F^2 - 2\frac{A+D}{2}F + (AD - BC) \right] = 0 \tag{95}$$

In order for there to be a non-trivial solution, the expression inside of the brackets must be equal to zero, and therefore F can be found by using the quadratic equation:

$$F_{\pm} = \frac{A+D}{2} \pm \left[\left(\frac{A+D}{2} \right)^2 + BC - AD \right]^{\frac{1}{2}} \tag{96}$$

Note that for an unstable cavity $(\frac{A+D}{2})^2 > AD - BC$, and so the solution is always real. The solution F_+ is used to describe a positive-branch unstable cavity. Positive branch means that there is no place in the cavity where the beam comes to a focus. The solution F_- is for a negative-branch unstable cavity. Negative branch means that there is one or more internal focal point. If F_+ *and* $F_- > 0$, then the cavity is a positive branch, and if F_+ *and* $F_- < 0$, then the cavity is a negative branch. The round-trip magnification for an unstable cavity is given by $M = \frac{r_1}{r_0}$, and therefore $M = F$. The fraction of photons that survive after one round trip is related to the magnification by $\Gamma = \frac{1}{M^2}$, and, noting that $F_+ = \frac{1}{F_-}$, then $\Gamma_+ = F_-^2$, $\Gamma_- = F_+^2$, and

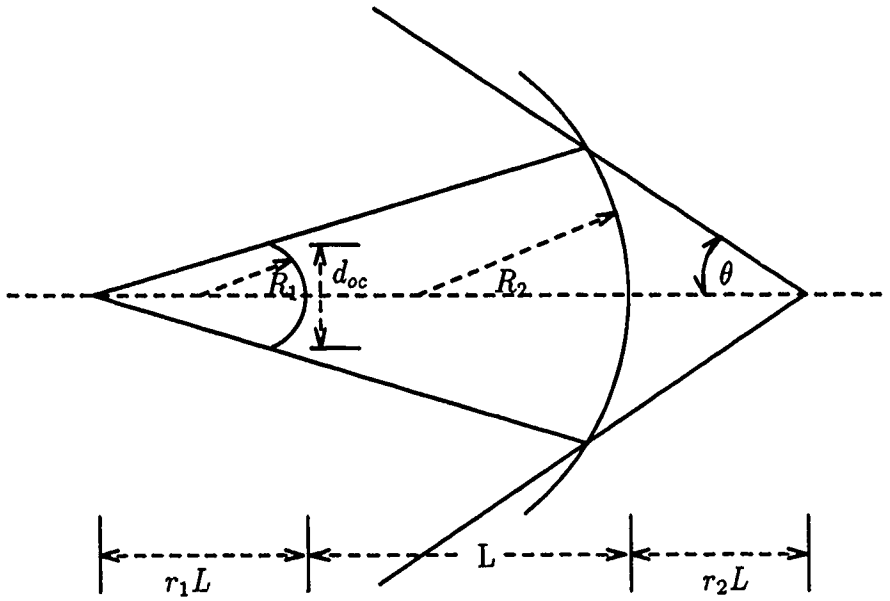

Figure 11. Equivalent Unstable Cavity

the fractional unstable out coupling $\delta = 1 - \Gamma$ (5).

Now, by using the round trip magnification and the diameter of the outcoupler d_{oc}, the spot size at the outcoupler can be found by $w_{oc} = d_{oc}\sqrt{M}$.

To find the divergence angle of the beam the following equations are used to transform the real cavity into a simplified equivalent cavity (10). For a general single-ended resonator (full round trip):

$A = 4g_1g_2 - 2g_2 - 1$

$B = 2g_2L$

$C = \frac{2}{L}(2g_1g_2 - g_1 - g_2)$

$D = 2g_2 - 1$ where

$g_1 = 1 - \frac{L}{R_1}$

$g_2 = 1 - \frac{L}{R_2}$

Knowing ABCD for the unstable cavity allows the determination of g_1, g_2 and L for an equivalent unstable cavity. Then from (5)

$$r_1 = \frac{[1-(g_1 g_2)^{-1}]^{\frac{1}{2}} - 1 + g_1^{-1}}{2 - g_1^{-1} - g_2^{-1}} \tag{97}$$

$$r_2 = \frac{[1-(g_1 g_2)^{-1}]^{\frac{1}{2}} - 1 + g_2^{-1}}{2 - g_1^{-1} - g_2^{-1}} \tag{98}$$

and by using Figure 11,

$$\theta = \arctan \frac{d_{oc}(r_1 + 1)}{2 r_1 r_2 L} \tag{99}$$

III. Validation of Model

3.1 Analytic Comparisons to Steady State Cases

The laser model can be broken into three distinct sections: thermal, rate equations, and cavity. In this section each of these will be validated by comparing them to special cases which have analytic solutions.

The first section to be validated will be the thermal model. By taking the limit as $t \rightarrow \infty$ the heat model will go to a steady state condition $\frac{dT}{dt} = 0$, and equation 53 can be written as

$$\nabla^2 T = -\frac{q^*(r)}{k} \tag{100}$$

$$\frac{d^2T}{dr^2} + \frac{1}{r}\frac{dT}{dr} = -\frac{q^*(r)}{k} \tag{101}$$

allowing $q^*(r) = Constant = q^*$ then

$$\frac{d}{dr}\left(r\frac{dT}{dr}\right) = -r\frac{q^*}{k} \tag{102}$$

and by direct integration

$$T = -\frac{r^2 q^*}{2k} + Cln(r) + D \tag{103}$$

Applying the boundary conditions:

$T(0) < \infty$

$\frac{dT(r)}{dr})_{r=R} = \frac{h}{k}(T(R) - T_{film})$

then C = 0 and

$D = T_{film} + \frac{Rq^*}{2h} + \frac{R^2 q^*}{4k}$

The solution can be written as

$$T(r) = T_{film} + \frac{q^*}{4k}\left[R^2 - r^2 + \frac{2kR}{h}\right] \tag{104}$$

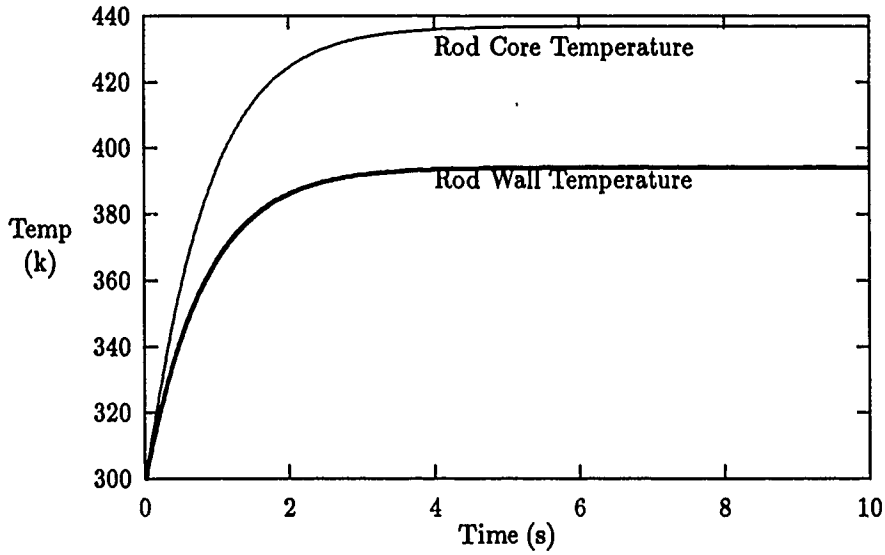

Figure 12. Rod Core and Wall Temperature Proceeding to the Steady State Limit

Figure 12 shows the temperature distribution of the rod core and the rod wall as a function of time. The data in Figure 12 was taken by using a flash lamp power of 10 kW, a power fraction for heat of 0.07, a pump duration of 10 s, water cooling with a velocity of 10 m/s, and a rod length of 0.1 m. The analytic solution for the temperature can be found by using equations 61, 62, and 104, yielding T(0) = 436.90 K and T(R) = 394.05 K, which matches the laser model exactly.

The analytic validation for the rate equations will proceed in a similar manner. As $t \rightarrow \infty$ then $\frac{d}{dt} = 0$ and equations 3 to 7 can be written as

$$\Phi \frac{\sigma c}{n}(N_2 - \frac{g_2}{g_1}N_1)\frac{l_r}{l_c} - \Phi \frac{\epsilon}{\tau_{rc}} + S = 0 \tag{105}$$

$$-\Phi \frac{\sigma c}{n}(N_2 - \frac{g_2}{g_1}N_1)f_2 - \frac{N_2}{\tau_{21}} + R_2' f_2 = 0 \tag{106}$$

$$\Phi \frac{\sigma c}{n}(N_2 - \frac{g_2}{g_1}N_1)f_1 + \frac{N_2}{\tau_{21}}\frac{f_1}{f_2} - \frac{N_1}{\tau_{10}} + R_1 f_1 = 0 \tag{107}$$

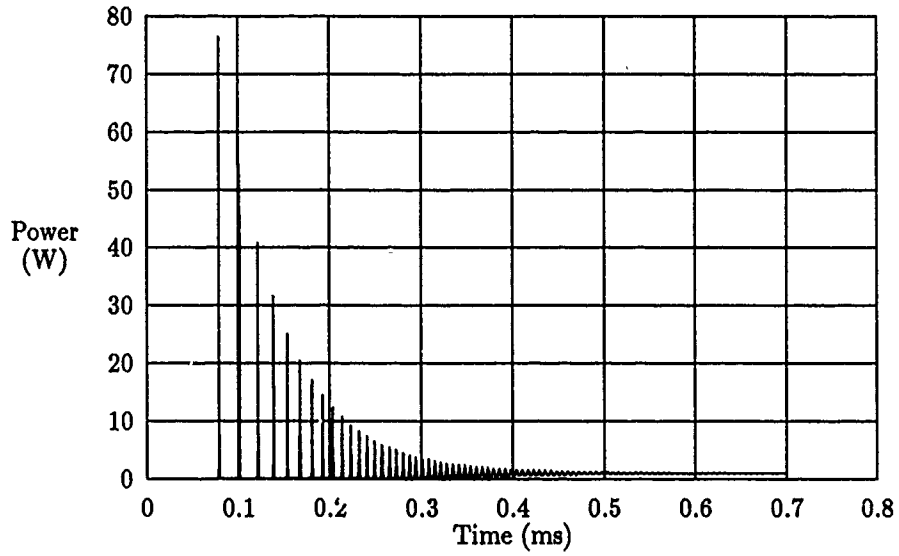

Figure 13. Continuous Wave Laser Proceeding to Steady State. Shown are the many relaxation oscillations before steady state is achieved.

$$\frac{N_1}{\tau_{10} f_1} + \frac{N_2}{\tau_{20} f_2} - R_1 - R_2' = 0 \tag{108}$$

In equation 105, S is very small and can be neglected. By using the definition $\epsilon \equiv \frac{\tau_{rc}}{\tau_{cav}}$, equation 105 can be written as

$$\frac{\sigma c}{n}(N_2 - \frac{g_2}{g_1} N_1)\frac{l_r}{l_c} = \frac{1}{\tau_{cav}} \tag{109}$$

Also, in equation 108, R_1 and $\frac{N_2}{\tau_{20} f_2}$ are small, and therefore equation 108 can be written as

$$N_1 = R_2' \tau_{10} f_1 \tag{110}$$

Now, substituting equation 109 into equation 106,

$$-\frac{\Phi \cdot l_c}{\tau_{cav} l_r} f_2 - \frac{N_2}{\tau_{21}} + R_2' f_2 = 0 \tag{111}$$

and substituting equation 110 into equation 109, then N_2 can be written as

$$N_2 = \frac{l_c}{l_r}\frac{n}{\sigma c}\frac{1}{\tau_{cav}} + R_2'\tau_{10}f_1 \tag{112}$$

Substituting equation 112 into equation 111 and solving for Φ,

$$\Phi = R_2'\tau_{cav}\frac{l_r}{l_c} - \frac{\tau_{cav}}{\tau_{21}f_2}\left[\frac{n}{\sigma c}\frac{1}{\tau_{cav}} + R_2'\tau_{10}f_1\frac{l_r}{l_c}\right] \tag{113}$$

The number of photons outcoupled into the beam is given by $\frac{d\Phi_{out}}{dt} = \frac{\Phi}{\tau_{fav}}$ and has units of photons per unit volume per second, and the outcoupled power is $P = \frac{d\Phi_{out}}{dt}h\nu$. Using equation 24 to find τ_{cav}, equation 49 to find τ_{fav}, equation 15 to find R_2', equation 1 to find f_1 and f_2, equation 41 to find σ, and also using Appendix C for τ_{21}, τ_{10}, n, ν, the steady state power per unit volume can be found.

As an example, using a cavity length of 0.2 m, a mirror 1 reflectivity of 0.9, a mirror 2 reflectivity of 0.98, a rod length of 0.1 m, a flash lamp power of 10 kW and a power fraction for lasing of 0.03 (see figure 13), the analytic value for the power is 83.4434 W/cc. Comparing that to the numerical value $\frac{PEAK\ POWER\ 0}{MODEV} = \frac{.97420}{.0117} = 83.2649 W/cc$ results in an error of 0.213 percent. This error is actually larger than the real error. The reason is that the final output of the peak power and mode volume from the model are truncated which produces round-off error. If this truncation error is removed, the numerical value is 83.4473 W/cc, and the error is only 0.0047 percent.

The last validation will be for the cavity by examining the divergence angle as it goes to the far-field limit. Figure 14 is a plot of the divergence angle for a stable cavity versus the distance from the outcoupler. The far-field divergence angle is given by $\theta = \frac{\lambda}{\pi w_o}$, where w_o is the radius of the spot at the beam waist. The far-field distance is given by $d_{ff} > \frac{a^2}{\lambda}$, where a is the diameter of the aperture, and λ is the wave length of the laser beam (18). Figure 14 was generated by using a cavity length of

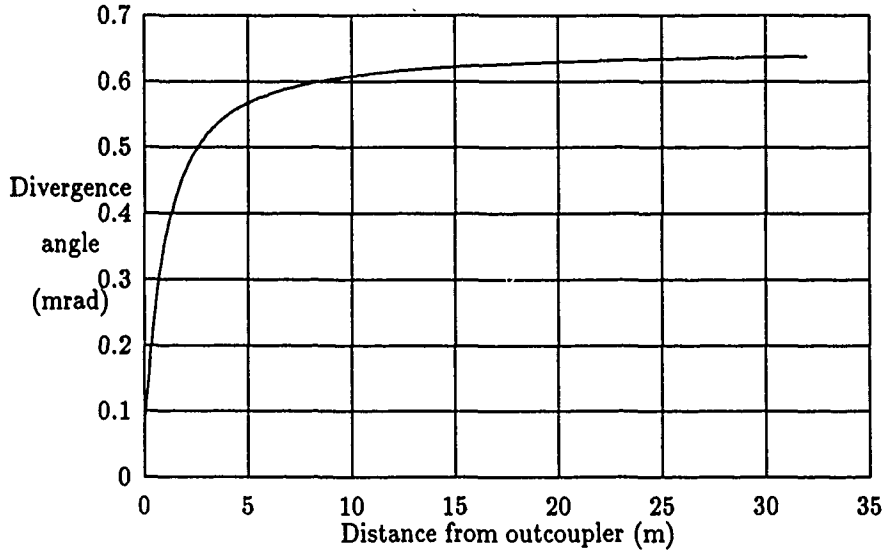

Figure 14. Divergence Angle as it Goes to the Far Field Limit.

0.2 m, a 10 m curvature for both mirrors, a rod length of 0.1 m and by varying target distance from 0 to 32 m. Using these inputs, the laser model produced a spot size on the outcoupler of 0.5234 mm. The spot size at the beam waist w_o is not known, but by letting w_0 equal the spot size on the outcoupler, a lower limit on the divergence angle can be found. Calculating the divergence angle yields $\theta = 0.6446\ mrad$. The model produces a divergence angle of $\theta = 0.6519\ mrad$, an error of only 1 percent. To calculate the far-field distance, the diameter of the outcoupling aperture must be found. Generally, the radius of the outcoupling aperture must be twice as large as the spot size to ensure that the entire transverse mode will emerge. Setting $a = 2.1296\ mm$, $d_{ff} = 4.08\ m$, which appears to be where the divergence angle in Figure 14 transitions to the far-field limit.

3.2 Comparison of Literature and Modeled Results

With a realistic model, it should be possible to match experimental data fairly accurately. The problem is that experimentalists don't usually give enough information to exactly match the experiment. This requires an educated "guess" of some of

the parameters.

The first attempt is to match (11) a single longitudinal mode, dye Q-switched laser. The single longitudinal mode was selected by an etalon which was made by placing a partially transmissive mirror between the laser rod and the back mirror. The parameters provided by the article are as follows:

6.4mm in diameter X 80mm Nd:YAG rod

30J flash lamp pulses

100μs pump duration

Outcoupling mirror reflectivity of 0.5

Outcoupling mirror radius of curvature 6.7m

Internal mirror reflectivity 0.85

Internal mirror flat

Back mirror reflectivity 1

Back mirror 3 flat

Cavity length of 77cm

Etalon length of 25cm

Total length (cavity + etalon) of 102cm

The results included an oscilloscope trace of a 20ns pulse which was matched very nicely by the model (see figure 15). Also reported was a 10ns pulse with an energy of 7mJ. By changing the model's Q-switch transmission to 0.6 an energy of 10mJ was produced. Therefore, the model has demonstrated the ability to predict single mode, Q-switched pulse shape and pulse energy fairly accurately.

The next attempt will be to match the results of a repetitively pulsed laser. Experimental data from (13) was reproduced fairly accurately (See figure 16).

The parameters provided by the article are as follows:

Water cooling

75mm X 6mm Nd:YAG rod

Cavity length of 600mm

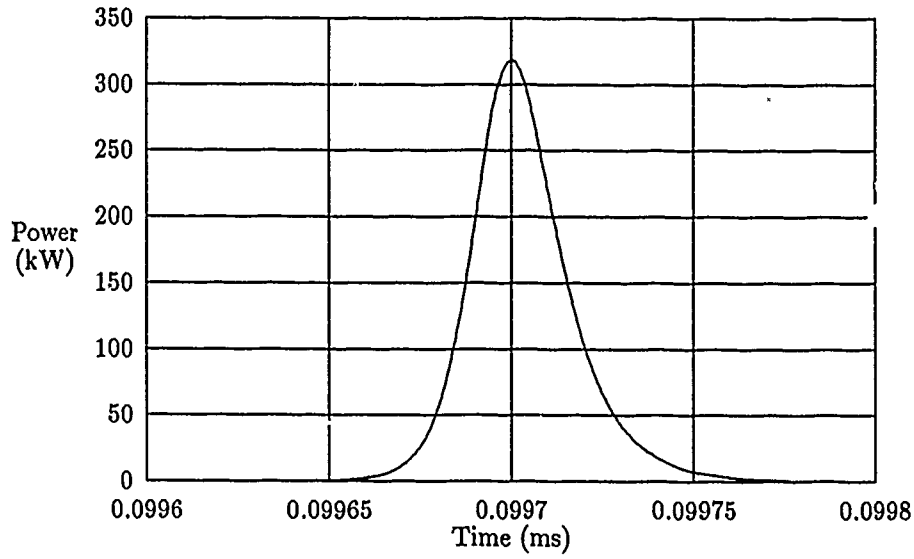

Figure 15. A Single Q-Switched Pulse that Matches an Oscilloscope Trace from (11)

Flat mirrors

2m converging lens to compensate for rod lensing

Outcoupling mirror reflectivity of 0.60

625Hz repetition rate

160kW input power

100μs pump duration

The reported energy in the first pulse was 35 mJ. By using the parameters provided, and by varying the Q-switch losses and the laser power fraction until the first pulse was approximately 35 mJ, the pulse trend was matched very well. The article reported a 12 percent change in the peak power between the 1st and the 40th pulse, and the model produced a 22 percent change. This could have been made to match the experimental results more closely by simply decreasing the model's water flow rate.

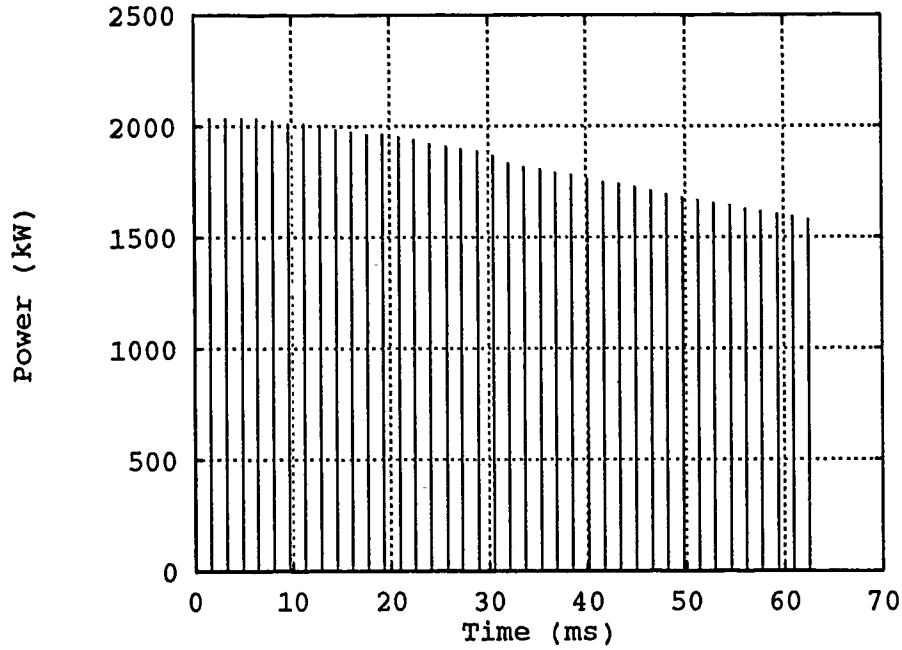

Figure 16. 40 Q-Switched Pulses that Match an Oscilloscope Trace from (13)

IV. Trend Analysis

4.1 Energy and Power vs. Output Coupling

Figures 17 and 18 describe the peak power and energy of a Q-switched laser versus outcoupling, for various input power settings. Similar plots can be found in (7) and they help to demonstrate that the model is working properly. Figures 17 and 18 were generated by varying the reflectivity of mirror 1 for the three different input power levels.

4.2 High Pulse Repetition Rate Transient Effects

In this section there will be a demonstration of the model's ability to represent a repetitively pulsed laser by exploring trends in the divergence angle, energy, and peak power.

Figure 19 is a plot of the divergence angle for each pulse in a 99 pulse train, for various repetition rates. For the 10 Hz case, there is a large increase in the divergence angle, and then it levels off. The reason for the sudden increase is that the rod is heated during the pump cycle and with the extended relaxation period between pulses the rod has a chance to cool. This cooling causes a radial temperature gradient in the laser rod which is responsible for producing thermal lensing. The curve flattens out because the rod reaches thermal equilibrium, i.e., the temperature gradient goes to a constant, and therefore the lensing of the rod becomes a constant. The 100 Hz case proceeds much like the 10 Hz case except the energy is deposited into the rod at a higher rate which causes the rod to heat up faster than the 10 Hz case. This increase in temperature coupled with the cooling time between pulses allows for a larger thermal gradient to develop. Finally, the 1000 Hz case initially rises much slower than the two previous cases. This is because a large number of pulses occur before a significant amount of heat can be removed from the rod wall

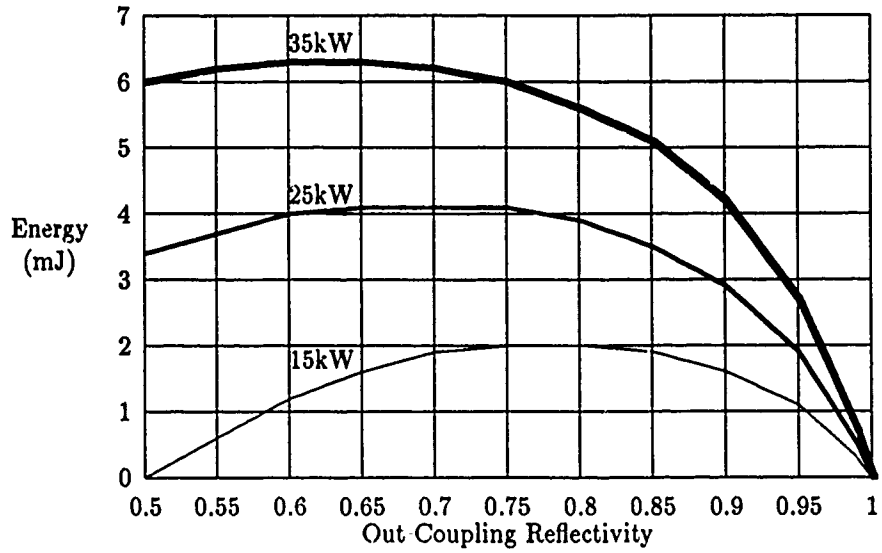

Figure 17. Energy Out vs. Outcoupling for a Single Pulsed Q-Switched Laser at Various Input Power Settings

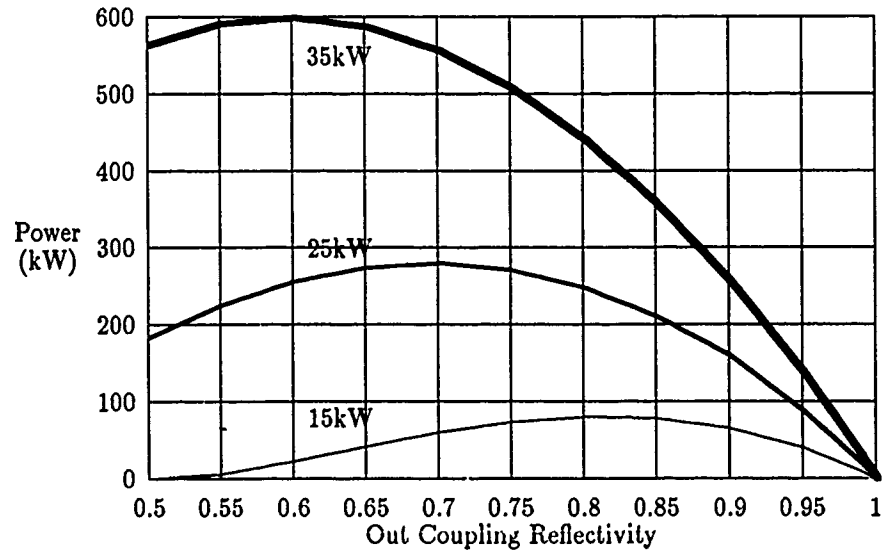

Figure 18. Peak Power vs. Outcoupling for a Single Pulsed Q-Switched Laser at Various Input Power Settings

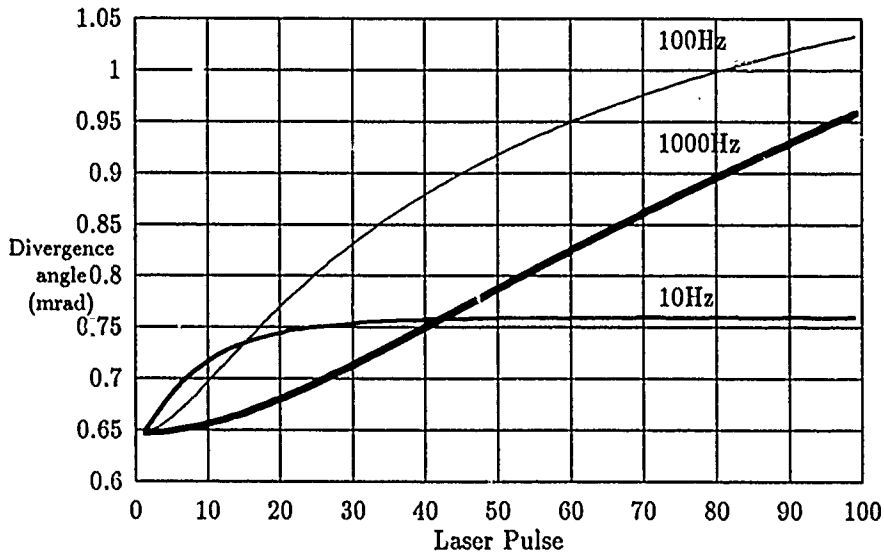

Figure 19. Divergence Angle vs. Laser Pulse for 10 J Input Energy and Various Repetition Rates.

and thus initially a significant thermal gradient is not produced. Note, the average temperature of the laser rod is higher for the 1000 Hz case than it is for the other two cases. This is because the total amount of energy deposited into the rod is the same for all cases, but in the 10 Hz and the 100 Hz cases, there is more time to cool between pulses than for the 1000 Hz case.

Figure 19 was generated by using a pump duration of 100 μs and a flash lamp power of 100 kW. The relaxation time was set to 0 μs for the 100 Hz case, to 9900 μs for the 100 Hz case, and to 99900 μs for the 10 Hz case.

Figure 20 very graphically shows the effect of cooling the laser rod. The top curve is the first pulse in a 40 pulse train; it is the same for all three cooling rates. Noting the trend in Figure 20, it can be seen that as the coolant flow rate is increased, the power in the 40th pulse decreases. This means that the higher the flow rate, the faster heat is removed from the surface of the laser rod, thus causing a larger radial thermal gradient. This causes lensing in the rod which serves to decrease the mode volume and therefore reduces the number of ions that contribute to the laser beam.

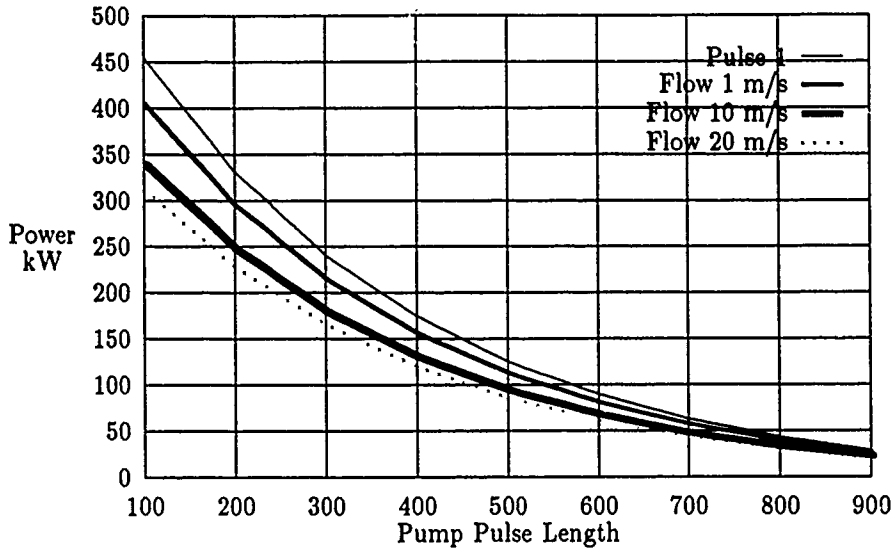

Figure 20. Trend of the 1st Pulse and the 40th Pulse for Three Different Coolant Velocity Settings. The first pulse is the same for all fluid velocities.

The total energy into the laser rod is a constant, and for the longer pulses, the flash lamp power decreases and therefore the pump rate decreases. This lower pump rate results in a smaller inversion even though the flash lamp is on for a longer time.

Figure 20 was made by varying pump duration, Q-switch delay, relaxation time and flash lamp power to keep the total input energy constant at 10 J and to hold the repetition rate constant at 1000 Hz.

Figure 21 is a plot of the peak power of the 40th pulse versus repetition rate. It was generated by using a pump duration of 1000 μs, a Q-switch delay of 999.5 μs, and by varying the relaxation time from 0 to 9000 μs for 15, 25, and, 35 kW input powers.

What can be seen from Figure 21 is that for very low repetition rates the laser rod has a chance to fully cool between laser pulses, but as the repetition rate increases there is less time for the laser rod to completely cool, allowing a thermal gradient to develop inside the rod. This thermal gradient is responsible for producing lensing which causes a reduction in the mode volume and thus a reduction in the

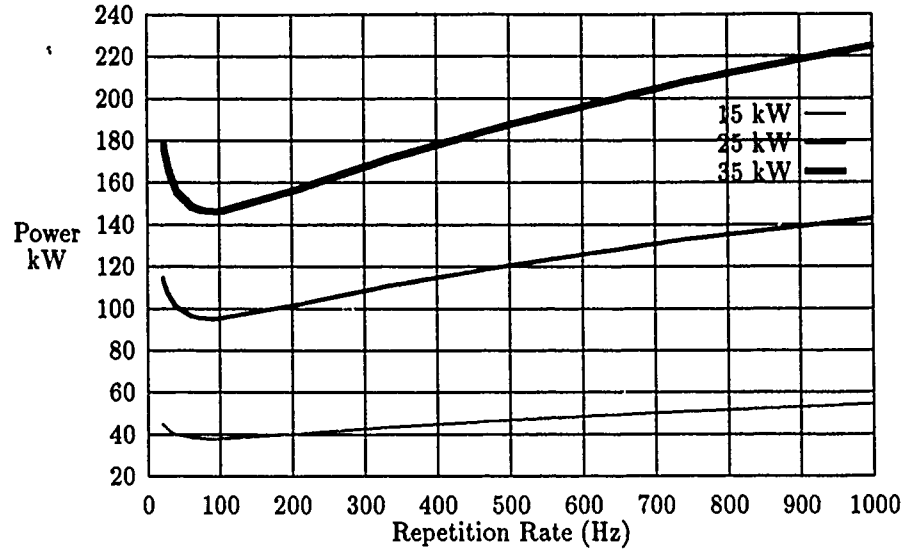

Figure 21. Peak Power vs. Repetition Rate for Various Input Powers and Constant Pump Duration of 1 ms

peak power. For higher repetition rates, the 40th pulse is produced before the laser rod develops a large thermal gradient, which translates into only a small decrease in mode volume. For the lower power settings the peak power is less sensitive to the repetition rate because there is less heating of the rod and only a small thermal gradient can develop.

The next case will examine the energy in the 40th pulse of a continuously pumped, Q-switched laser (see Figure 22). At the low repetition rates, there is a significant amount of thermal lensing, because the lamp has been on for a long period of time allowing a large thermal gradient to develop which causes a reduction in mode volume. As the pulse rate increases, the 40th pulse can emerge from the cavity before the rod can develop a significant thermal gradient. Once again, the curve begins to fall off because there isn't enough time between pulses to fully populate the upper laser level, causing a decrease in the output energy. The sudden rise is from inversion left over from the 39th pulse. If the inversion isn't high enough for the 39th pulse to lase then the inversion will contribute to the 40th pulse. The sudden drop is because the 40th pulse has become the pulse without enough inversion to lase.

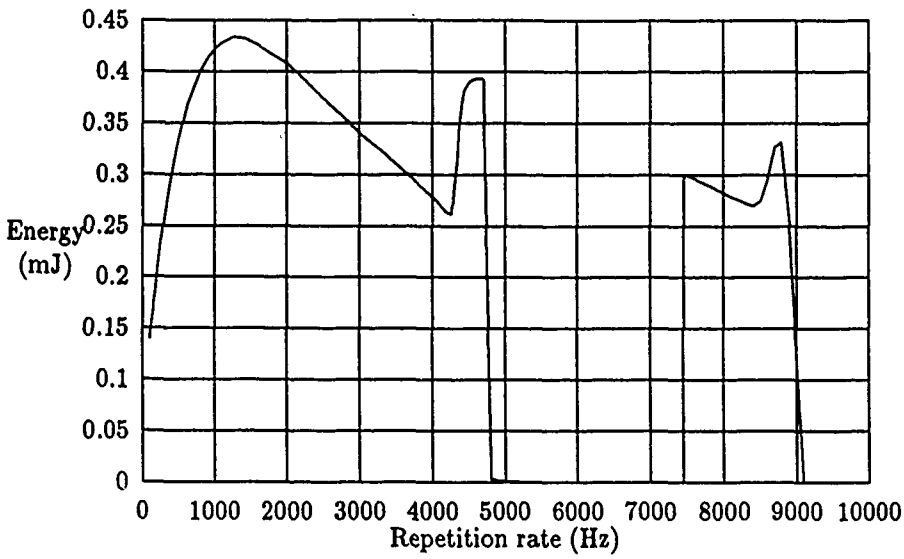

Figure 22. Energy in the 40th Pulse vs. Repetition Rate.

Figure 22 was generated by using a flash lamp power of 10 kW, a relaxation time of 0, and by varying the pump duration from 100 to 10000 μs. A relaxation time of 0 means that the flash lamp will not be turned off between pulses.

V. Conclusion

5.1 Conclusion

By modeling the laser rate equations, the cavity design, and the temperature distribution in the rod, it is possible to do an accurate job of describing an Nd:YAG laser for both continuous wave and pulsed operation. Each piece is necessary to accurately represent the laser. The rate equations are responsible for producing the detailed laser pulse shape and for producing the outputs of power and energy. The rate equations are limited in that they can only produce energy and power on a per unit volume basis. The cavity model is included to calculate the fraction of rod volume that contributes to the beam, making absolute energy and power calculations possible. To model the cavity properly, the thermal lensing of the laser rod needed to be included. This lensing has a significant effect on the mode volume and therefore has a significant effect on the energy and power predicted by the model.

5.2 Suggested Improvements

While coding the laser model, a QuickBASIC limit was discovered. QuickBASIC is limited to a maximum module size of 64K, which ultimately prevented the addition of new material to the laser model. In order to allow future expansion of the model, the code would need to be broken into smaller modules.

After the code is broken into smaller modules, the first addition should be a more realistic Q-switch. Presently the Q-switch goes from off to on instantaneously and stays open until the end of the integration of the pulse. A more realistic Q-switch should include a finite opening and closing time.

The present unstable cavity code does not give any information about the beam inside the cavity. This lack of information means that an accurate evaluation of the mode volume can not be determined. Presently a mode volume equal to the size of

the laser rod is assumed. This is not a good assumption and therefore the energy and power for the unstable cavity design is somewhat questionable.

A very difficult addition would be a realistic flash lamp model. This addition is not needed for the Nd ion laser but, if there is a future desire to extend the code to other laser materials then this would be an important modification.

The last set of improvements are all related to temperature dependence. The first is thermally induced birefringence. As the rod develops a radial temperature gradient, stress is produced inside the laser rod. This stress produces birefringence effects. Thermally induced birefringence is as much a design consideration as the thermal lensing of the laser rod and should be added to more completely model the Nd laser.

The stress that produces the birefringence, in extreme cases, can also cause the laser rod to fracture. These laser rod stress limits should be added to make very high energy laser pulse evaluations more realistic. Another thermal effect is the laser rod expansion along the lasing axis. This lengthening of the rod affects the laser cavity's design and therefore the cavity's stability. And finally, temperature changes in the laser rod produce shifts in the laser frequency. Tracking the changes in the frequency would be useful in matching the laser output to detectors in applications such as laser radar.

Appendix A. **Numerical Techniques**

The model uses an Adams predictor-corrector method to solve the differential equations in chapter 2. Because this method requires a set of initial data points, a fourth order Runge-Kutta integration routine is used to start the Adams predictor corrector routine.

The fourth order Runge-Kutta technique uses the following algorithm (3):

Define the rate equations as functions to be called by the integration routines.

$$F_1(\phi, n_1, n_2, n_3) = \phi(n_2 - \frac{g_2}{g_1} n_1) - \phi + s \tag{114}$$

$$F_2(\phi, n_1, n_2, n3) = \phi(n_2 - \frac{g_2}{g_1} n_1) f_1 \frac{l_c}{l_r} + \frac{n_2}{t_{21}} \frac{f_1}{f_2} + \frac{n_3}{t_{31}} f_1 - \frac{n_1}{t_{10}} + r_1 f_1 \tag{115}$$

$$F_3(\phi, n_1, n_2, n3) = -\phi(n_2 - \frac{g_2}{g_1} n_1) f_2 \frac{l_c}{l_r} + \frac{n_3}{t_{32}} f_2 - \frac{n_2}{t_2} + r_2 f_2 \tag{116}$$

$$F_4(\phi, n_1, n_2, n3) = -\frac{n_3}{t_3} + r_3 \tag{117}$$

Starting with the following initial conditions

$$0 \leq t \leq b \quad n_1(0) = 0 \quad n_2(0) = 0 \quad n_3(0) = 0 \quad \phi(0) = 0 \tag{118}$$

where b = the time to integrate to and δt = the incremental time step.

Set N = $\frac{b}{\delta t}$

Set t = 0

Loop N times to integrate to time b

Loop i from 1 to 4

Set $K_{1i} = \delta t F_i(\phi, n_1, n_2, n_3)$

Loop i from 1 to 4

Set $K_{2i} = \delta t F_i(\phi + \frac{K_{11}}{2}, n_1 + \frac{K_{12}}{2}, n_2 + \frac{K_{13}}{2}, n_3 + \frac{K_{14}}{2})$

Loop i from 1 to 4

Set $K_{3i} = \delta t F_i(\phi + \frac{K_{21}}{2}, n_1 + \frac{K_{22}}{2}, n_2 + \frac{K_{23}}{2}, n_3 + \frac{K_{24}}{2})$

Loop i from 1 to 4

Set $K_{4i} = \delta t F_i(\phi + K_{31}, n_1 + K_{32}, n_2 + K_{33}, n_3 + K_{34})$

Set $\phi' = \phi + \frac{K_1+2(K_2+K_3)+K_4}{6}$

Set $n_1' = n_1 + \frac{K_1+2(K_2+K_3)+K_4}{6}$

Set $n_2' = n_2 + \frac{K_1+2(K_2+K_3)+K_4}{6}$

Set $n_3' = n_3 + \frac{K_1+2(K_2+K_3)+K_4}{6}$

set t' = t + δt

The primed quantities are the values at the time t'.

The Runge-Kutta routine is very capable and could have been used exclusively to integrate the set of differential equations. The problem with the routine is that it is very slow. Also, it is only a fourth-order routine, which means that a very small time step is needed to accurately integrate the rate equations. The small time step translates into a very large number of points, a lot of computation time to calculate the points, and a lot of storage space to store the points. To get around these limitations, the Runge-Kutta routine is only used to initiate a sixth-order Adams predictor-corrector routine. The sixth-order routine allows a larger time step to be used and still achieve the same accuracy as the Runge-Kutta routine. Also, the Adams method is, by design, a faster technique. Therefore, there is a two-fold speed increase by employing this routine.

There is a problem with initiating a sixth-order routine with a fourth-order routine. The lower accuracy of the starting routine could introduce error into the integration. This problem is overcome by running the Runge-Kutta routine with a time step of $\frac{\delta t}{2}$ and using every other point generated to start the Adams routine.

The following is the Adams predictor-corrector algorithm (4):
Call the Runge-Kutta routine 10 times with a time step of $\frac{\delta t}{2}$ and use the 0th, 2nd, 4th, 6th, 8th, and 10th points to start the Adams routine.

Set N = $\frac{b}{\delta t}$

Set $t = 5\delta t$

Loop i from 6 to N to integrate to time b

Predict

Set $\phi' = \phi(t) + \delta t[\frac{4277}{1440}F_1(t) - \frac{7923}{1440}F_1(t-\delta t) + \frac{9982}{1440}F_1(t-2\delta t) - \frac{7298}{1440}F_1(t-3\delta t) + \frac{2877}{1440}F_1(t-4\delta t) - \frac{475}{1440}F_1(t-5\delta t)]$

Set $n_1' = n_1(t) + \delta t[\frac{4277}{1440}F_2(t) - \frac{7923}{1440}F_2(t-\delta t) + \frac{9982}{1440}F_2(t-2\delta t) - \frac{7298}{1440}F_2(t-3\delta t) + \frac{2877}{1440}F_2(t-4\delta t) - \frac{475}{1440}F_2(t-5\delta t)]$

Set $n_2' = n_2(t) + \delta t[\frac{4277}{1440}F_3(t) - \frac{7923}{1440}F_3(t-\delta t) + \frac{9982}{1440}F_3(t-2\delta t) - \frac{7298}{1440}F_3(t-3\delta t) + \frac{2877}{1440}F_3(t-4\delta t) - \frac{475}{1440}F_3(t-5\delta t)]$

Set $n_3' = n_3(t) + \delta t[\frac{4277}{1440}F_4(t) - \frac{7923}{1440}F_4(t-\delta t) + \frac{9982}{1440}F_4(t-2\delta t) - \frac{7298}{1440}F_4(t-3\delta t) + \frac{2877}{1440}F_4(t-4\delta t) - \frac{475}{1440}F_4(t-5\delta t)]$

Correct

Set $\phi'' = \phi(t) + \delta t[\frac{475}{1440}F_1(t+\delta t) + \frac{1427}{1440}F_1(t) - \frac{798}{1440}F_1(t-\delta t) + \frac{482}{1440}F_1(t-2\delta t) - \frac{173}{1440}F_1(t-3\delta t) + \frac{27}{1440}F_1(t-4\delta t)]$

Set $n_1'' = n_1(t) + \delta t[\frac{475}{1440}F_2(t+\delta t) + \frac{1427}{1440}F_2(t) - \frac{798}{1440}F_2(t-\delta t) + \frac{482}{1440}F_2(t-2\delta t) - \frac{173}{1440}F_2(t-3\delta t) + \frac{27}{1440}F_2(t-4\delta t)]$

Set $n_2'' = n_2(t) + \delta t[\frac{475}{1440}F_3(t+\delta t) + \frac{1427}{1440}F_3(t) - \frac{798}{1440}F_3(t-\delta t) + \frac{482}{1440}F_3(t-2\delta t) - \frac{173}{1440}F_3(t-3\delta t) + \frac{27}{1440}F_3(t-4\delta t)]$

Set $n_3'' = n_3(t) + \delta t[\frac{475}{1440}F_4(t+\delta t) + \frac{1427}{1440}F_4(t) - \frac{798}{1440}F_4(t-\delta t) + \frac{482}{1440}F_4(t-2\delta t) - \frac{173}{1440}F_4(t-3\delta t) + \frac{27}{1440}F_4(t-4\delta t)]$

set t' = t + δt

The primed quantities are the predicted values and the double primed quantities are the corrected values at time t'. A useful benefit from the routine is that the corrector portion is closed-form, making it possible to iterate the corrector section to increase the accuracy. The laser model utilizes this feature to produce better results.

Appendix B. Code Instructions

B.1 User Input

Insert floppy into drive A:

type A: *return*

type Nd *return*

Select the number pad operational

Push 2 to move the highlight bar up and push 8 to move the highlight bar down.

Press *return* to select the highlighted option.

Again press 2 and 8 to move up and down until the proper choice is highlighted and press *return*. Input the new value at the prompt and proceed as above to the next value to change.

When all parameters are set then highlight RUN MODEL and press *return* to run the code.

CAVITY

Cavity Length

Must be longer than the laser rod

Mirror 1

This is the reflectivity of the outcoupling mirror. The reflectivity is restricted to the range of 0.1 to 0.99999.

Mirror 2

This is the reflectivity of the back mirror and is restricted to the range of 0.1 to 0.99999.

Q-Switch Trans

This is the single-pass transmission of the Q-Switch and ranges from 0.1 to 0.99999.

Curvature Mirror 1

The radius of curvature of the outcoupling mirror and its value can range from -1E10 to +1E10.

Curvature Mirror 2

The radius of curvature of the back mirror and its value can range from -1E10 to +1E10.

Diameter Mirror 1

Diameter of the outcoupling mirror. Only used during unstable cavity calculations. Its value must be greater than zero.

Target Distance

This is the distance to some arbitrary target and is used to calculate the laser spot size on target.

ROD-COOLANT

Rod Length

Must be less than the length of the cavity and greater than zero.

Rod Radius

The radius of the laser rod, and must be greater than zero.

Curvature Rod Ends

The radius of curvature at the ends of the laser rod. Can range from -1E10 to +1E10.

Laser Material

This is the material the laser rod is made of where 1 = Nd:YAG, 2 = Nd:Silicate "ED-2", and 3 = Nd:Phosphate "Q-88".

Percent Nd: Ions

Percentage of Nd: Ions in the laser rod and must be greater than zero.

Coolant Velocity

The velocity that the cooling fluid flows over the laser rod. Its value must be greater

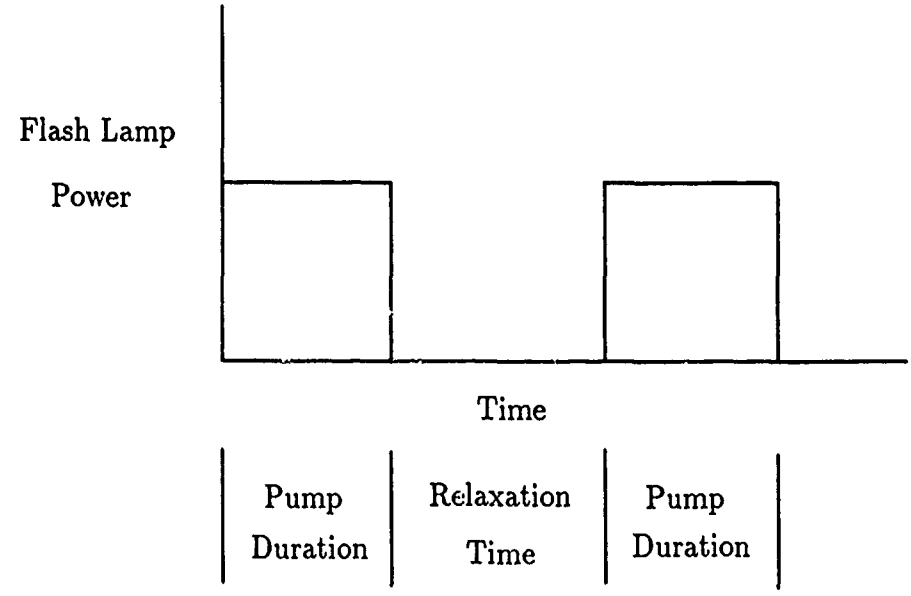

Figure 23. Flash Lamp Duty Cycle

than zero.

Coolant

This selects the cooling fluid where 1 = Water and 2 = Dry Air.

Coolant Temperature

This is the bulk temperature of the cooling fluid. It is also the temperature of the laser rod. The coolant temperature range is different for the two different cooling fluids. For water the temperature range is from 273 K to 600 K, and for air the temperature range is from 223 K to 2500 K.

FLASH LAMP

Pump Duration

The length of time that the flash lamp is turned on (see Figure 23). NOTE: (Pump Duration + Relaxation Time) must be greater than or equal to the (Q-Switch Delay + Integrate to).

Q-Switch Delay

The delay from the time the flash lamp is turned on to the time the Q-switch is

opened. By setting this value to zero the losses from the Q-switch are neglected. This has the same effect as removing the Q-switch from the cavity. NOTE: (Q-Switch Delay + Integrate to) must be less than or equal to (Pump Duration + Relaxation Time).

Relaxation Time

The length of time from flash lamp turn-off to flash lamp turn-on (see Figure 23). NOTE: (Pump Duration + Relaxation Time) must be greater than or equal to the (Q-Switch Delay + Integrate to).

Flash Lamp Power

The electrical power into the flash lamp or diode pump array. This value must be greater than zero.

Power Fraction Laser

The fraction of flash lamp electrical power that goes into the laser. A typical value for a flash lamp is about 0.03, and a typical value for a diode pump source is about 0.2.

Power Fraction Heat

The fraction of flash lamp electrical power that goes into heating the laser rod. A typical value for a flash lamp is about 0.07, and a typical value for a diode pump source is about 0.2.

INTEGRATION

Number of pulses

The number of laser pulses to be integrated. The value must be an integer ranging from 1 to 100.

Integrate to

"Integrate to" always starts from the time the Q-Switch is opened and is the amount of time the integrator will integrate. This value must be greater than zero and is

typically set between .5 and 1 for most Q-Switched pulses, but can range as high as 100 to 150 for CW operation.

Step Size

This is the incremental step size that the integrator will use to integrate the laser pulse. The smaller the step size, the more accurately the laser pulse is integrated, but the cost is a longer wait for the output. Also, the smaller the step size, the larger the number of points needed to integrate the pulse. This value should not be greater than 0.7 for CW operation and not greater than 0.2 for Q-Switch operation. These limits will help eliminate the OVERFLOW error by the computer.

File Storage Path

This is the path name the model will use to locate/save the four data files created. i.e. "C:/", "D:/","C:/SUBDIRECTORY/" etc. Disregard the quotation marks in these examples.

Mode of Operation

This is a simple switch that determines Q-Switch operation versus Continuous Wave operation. 1 = Q-Switch and 2 = CW. NOTE: When CW is selected, the heat model just produces the steady state temperature distribution inside the laser rod. Also, when CW is selected (Pump Pulse = Integrate to), the Q-switch delay and the relaxation time are set to 0.

Store Power File

This is a simple switch that determines if the power file will be saved to disk; 1 = Yes and 2 = No. When a large number of pulses are integrated, the power file can become quite large, taking up a lot of storage space, and storing the power file is not advisable. If the power file is not saved then the two power plots can not be displayed.

Number Of Points

This is not an input but by setting the (Step Size) and (Integrate to) the value

changes. This value should not exceed 10000 for a single pulse. Exceeding 10000 points in a single pulse will produce a SUBSCRIPT OUT OF RANGE error.

B.2 Model Output

After running the model the default output is information about each laser pulse. To continue on past this point press *Return* until the main menu returns. Once the model has been run, a new menu item appears, PLOT DATA. By selecting PLOT DATA another menu appears. The first entry is

Temp vs Time

This will produce a plot of the rod core and the rod wall temperature with respect to time. To exit back to the menu, press *Return* twice.

Power vs Time

This is a plot of laser power with respect to time for all laser pulses. To exit back to the menu press *Return* twice. This will not be displayed if the store power file option was set to NO.

Pulse P vs T

This is a plot of the laser power for each individual pulse. To exit back to the menu press *Return* once and answer no. This will not be displayed if the store power file option was set to NO.

Pulse Data

This is the same information that is displayed when the code finishes running a case. Below is a description of what these outputs mean.

Shell to Dos

This option allows the user to temporarily exit the code and use DOS commands. When the user is finished the model can be reentered by typing **exit** followed by *return.*

The following is a description of the information displayed by the Pulse Data option.

PULSE

Identifies the pulse number.

STABILITY

This has three possible outputs: Stable, Positive, and Negative. Stable means that the laser cavity was stable for the laser pulse, Positive means positive branch unstable cavity, and Negative means negative branch unstable cavity.

STABILITY

This is the numerical value for stability and generally must be less than two for the cavity to be stable.

ENERGY 0,0

The energy in the laser pulse for the 0,0 transverse mode. The units are Joules.

PEAK PWR 0,0

The peak power of the laser pulse for the 0,0 transverse mode. The units are Watts.

ENERGY p,0

The energy in the laser pulse for the p,0 transverse mode. The units are Joules.

PEAK PWR p,0

The peak power of the laser pulse for the p,0 transverse mode. The units are Watts.

FWHM

Full-width at half-maximum of the laser pulse power. The units are seconds.

PULSE START

This is the real-time start of the laser pulse, and is used to help isolate the pulse when plotting. This value is meaningless for CW operation.

PULSE END

This is the real-time end of the laser pulse, and is used to help isolate the pulse when

plotting. This value is meaningless for CW operation.

TEMP r=0

The temperature of the laser rod core during the laser pulse in Kelvins.

TEMP r=0

The temperature of the laser rod wall during the laser pulse in Kelvins.

SPOT M1

Spot size radius on the outcoupling mirror in millimeters.

SPOT M2

Spot size radius on the back mirror in millimeters.

SPOT min

Minimum spot size radius inside the laser rod in millimeters.

SPOT max

Maximum spot size radius inside the laser rod in millimeters.

MODEV 0,0

Volume of the laser rod used by the 0,0 laser mode in cubic centimeters.

MODE p,0

Indicates the highest order transverse mode that the laser can operate in where p=mode.

MODEV P,0

Volume of the laser rod used by the P,0 laser mode in cubic centimeters.

SPOT oc

Spot size radius at the outcoupling mirror outside the cavity in millimeters.

SPOT TARGET

Spot size radius on target in meters.

SSGain

Small-signal gain in the laser rod at the start of the Q-switched pulse in cm^{-1}.

UNSTAB OUT

Fractional outcoupling for an unstable cavity.

Dvrg anle

Beam divergence angle in milliradians.

Rod Condition

There two possible outputs including GOOD and MELTED.

There are also four output files stored on disk. These files are stored according to the path specified on the input screen. The first file is titled "Input.dat", this file contains a snapshot of the input screen. The second file is titled "Pulse.dat" and contains the same information displayed by the pulse data option. The third file is named "TmpTme.dat" and contains the laser rod temperature information. The information is stored in the format Time (ms), Rod Core Temp (K), Rod Wall Temp (K). The last file is named "Pow.dat" and holds the power information in the format Time (ms), Power (kW).

Appendix C. **Table of Constants**

Table 6. Laser Material Constants along with the Source Reference.

Materieal	Nd:YAG	Nd:Sil ED-2	Nd:Phos Q-88
Scatter losses by rod (/m)	.2	.3	.3
Einstein A_{21} coefficient (/s)	820	1380	1941 [1]
τ_{10} (s)	$1x10^{-8}$	$1.25x10^{-9}$	$1.25x10^{-9}$ [1]
τ_{20} (s)	∞ [1]	∞ [1]	∞ [1]
τ_{21} (s)	$2.3x10^{-4}$	$2.3x10^{-4}$ [1]	$2.3x10^{-4}$ [1]
τ_{30} (s)	∞ [1]	∞ [1]	∞ [1]
τ_{31} (s)	∞ [1]	∞ [1]	∞ [1]
τ_{32} (s)	$1x10^{-8}$	$1x10^{-8}$ [1]	$1x10^{-8}$ [1]
Index of Refraction	1.82	1.5554	1.5310
Laser Frequency Hz	$2.8172045x10^{14}$	$2.8220841x10^{14}$	$2.8443074x10^{14}$
Line Width Hz	$1.4985x10^{11}$	$7.400736x10^{12}$	$5.829511x10^{12}$
Energy Levls in Manafold 1	6	2	2
Energy of level 1 /cm	0	0	0
Degeneracy of level 1	2	4 [1]	4 [1]
Energy of level 2 /cm	26	310 [1]	310 [1]
Degeneracy of level 2	2	8 [1]	8 [1]
Energy of level 3 /cm	108	-	-
Degeneracy of level 3	2	-	-
Energy of level 4 /cm	146	-	-
Degeneracy of level 4	2	-	-
Energy of level 5 /cm	459	-	-
Degeneracy of level 5	2	-	-
Energy of level 6 /cm	512	-	-
Degeneracy of level 6	2	-	-
Energy level transitioned to	3	1	1

[1]Warning: An experimental value could not be found. The value given is only a "reasonable" approximation of the real value.

Table 7. Laser Material Constants along with the Source Reference Continued.

Materieal	Nd:YAG	Nd:Sil ED-2	Nd:Phos Q-88
Energy Levls in Manafold 2	2	2	2
Energy of level 1 /cm	0	0	0
Degeneracy of level 1	2	2	2
Energy of level 2 /cm	84	110 [1]	110 [1]
Degeneracy of level 2	2	2	2
Energy level transitioned from	2	1	1
Conductivity $\frac{W}{m-K}$	13	1.255	.73638
Specific Heat $\frac{W-s}{kg-K}$	590	920.48	878.64
Density $\frac{kg}{m^3}$	4560	2510	2670
$\frac{dn}{dT}$ /K	$7.3x10^{-6}$	$3.8x10^{-6}$	$-5.0x10^{-7}$
Melting Point K	2243 [1]	1000 [1]	1000 [1]
Source	(5) (7) (8) (14) (15)	(7) (16)	(7) (16)

Bibliography

1. Dance, Brian. Nd:YAG Based Camera "Sees" in Murky Water. *Laser Focus,* 28 (June 1987).
2. Chapman, Alan J. *Heat Transfer Fourth Edition.* Macmillan Publishing Company, 1974.
3. Burden, Richard L., Faires, Douglas L. and Reynolds, Albert C. *Numerical Analysis Second Edition.* Prindle, Weber and Schmidt, 1978.
4. Hornbeck, Robert W. *Numerical Methods* Quantum Publishers Inc., 1975.
5. Verdeyen, Joseph T. *Laser Electronics Second Edition* Prentice Hall, 1981.
6. Pitts, Donald R., Sissom, Leighton E. *Heat Transfer Schaum's Outline Series* McGraw-Hill Publishing Company, 1977.
7. Koechner, Walter *Solid-State Laser Engineering* Springer-Verlag, 1988.
8. Foster, J. D., Osterink, L. M. "Thermal Effects in a Nd:YAG Laser" *Journal of Applied Physics*, Vol. 41, No. 9, 3656-3663, 1970.
9. Metcalf, David, de Giovanni, Pascal, Zachorowski, Jerzy, and Leduc, Michele "Laser Resonators Containing Self-Focusing Elements" *Applied Optics*, Vol. 26, No. 21, 4508-4517, 1987.
10. Siegman, Anthony E. "A Canonical Formulation for Analyzing Multielement Unstable Resonators", *IEEE Journal of Quantum Electronics*, Vol. QE-21, No. 1, 1976.
11. Voss, D. F., Goldberg, L. S. "Simple Single Longitudinal Mode Q-Switched Nd:YAG Oscillator" *IEEE Journal of Quantum Electronics*, Vol. QE-21, No. 2, 1985.
12. Tarasov, L. V. *Laser Physics*, Mir Publishers, 1983.
13. Knight, R. C., Dewhurst, R. J., and Ramsden, S. A. "Efficient Burst-Mode Operation of a Very High Repetition-Rate Nd:YAG Laser" *Journal of Physics E*, Vol. 13, 1339-1342, 1980.
14. Kushida, T., Kinoshita, S., Ohtsuki, T., and Yamada, T. "Multiphonon Relaxation Ratio from Pumped Level to Upper Laser Level in YAG:Nd" *Solid State Communications*, Vol. 44, No. 9, PP 1363-1365, 1982.
15. Singh, S., Smith, R. G., and Van Uitert, L. G. "Stimulated-Emission Cross Section and Florescent Quantum Efficiency of Nd in Yttrium Aluminum Garnet at Room Temperature", *Physical Review B* Vol. 10, No. 6, pp 2566-2572, 1974.
16. Brown, D. C. *High-Peak-Power Nd:Glass Laser Systems* Springer-Verlag, 1981.

17. Fan, Tso Yee "Effect of Finite Lower Level Lifetime on Q-Switched Lasers" *IEEE Journal of Quantum Electronics* Vol. 24, No. 12, 1988.

18. Hecht, Eugene *Optics second edition*, Addison-Wesley Publishing Company, 1987.

SECURITY CLASSIFICATION OF THIS PAGE

REPORT DOCUMENTATION PAGE

Form Approved OMB No. 0704-0188

1a. REPORT SECURITY CLASSIFICATION: UNCLASSIFIED	1b. RESTRICTIVE MARKINGS
2a. SECURITY CLASSIFICATION AUTHORITY	3. DISTRIBUTION/AVAILABILITY OF REPORT: UNLIMITED
2b. DECLASSIFICATION/DOWNGRADING SCHEDULE	
4. PERFORMING ORGANIZATION REPORT NUMBER(S): AFIT/GEP/ENP/90D-5	5. MONITORING ORGANIZATION REPORT NUMBER(S)
6a. NAME OF PERFORMING ORGANIZATION: SCHOOL OF ENGINEERING; 6b. OFFICE SYMBOL (If applicable)	7a. NAME OF MONITORING ORGANIZATION
6c. ADDRESS (City, State, and ZIP Code): AIR FORCE INSTITUTE OF TECHNOLOGY WRIGHT PATTERSON AFB OH, 45433-6506	7b. ADDRESS (City, State, and ZIP Code)
8a. NAME OF FUNDING/SPONSORING ORGANIZATION; 8b. OFFICE SYMBOL (If applicable)	9. PROCUREMENT INSTRUMENT IDENTIFICATION NUMBER
8c. ADDRESS (City, State, and ZIP Code)	10. SOURCE OF FUNDING NUMBERS: PROGRAM ELEMENT NO. / PROJECT NO. / TASK NO. / WORK UNIT ACCESSION NO.

11. TITLE (Include Security Classification)

CONTINUOUS WAVE AND PULSED SOLID STATE LASER MODEL

12. PERSONAL AUTHOR(S)

ROTONDARO, MATTHEW DON

13a. TYPE OF REPORT	13b. TIME COVERED	14. DATE OF REPORT (Year, Month, Day)	15. PAGE COUNT
MASTERS THESIS	FROM _____ TO _____	1990 NOVEMBER	77

16. SUPPLEMENTARY NOTATION

17. COSATI CODES			18. SUBJECT TERMS (Continue on reverse if necessary and identify by block number)
FIELD	GROUP	SUB-GROUP	Nd:YAG
			MODEL

19. ABSTRACT (Continue on reverse if necessary and identify by block number)

A solid state laser is modeled for use on a personal computer. The model can accurately represent Nd:YAG and Nd:Glass lasers during both continuous wave and repetitively pulsed operation. The large number of input variables allow the user to make changes to the cavity, optical pump source, and the cooling system. The model calculates the energy, power, and divergence angle of the beam along with other variables. Because of its user-friendly interface, it is possible for someone with limited laser experience to obtain useful information. (THESES. / JHD)

20. DISTRIBUTION/AVAILABILITY OF ABSTRACT	21. ABSTRACT SECURITY CLASSIFICATION
XX UNCLASSIFIED/UNLIMITED ☐ SAME AS RPT. ☐ DTIC USERS	UNCLASSIFIED
22a. NAME OF RESPONSIBLE INDIVIDUAL: MATTHEW D. ROTONDARO	22b. TELEPHONE (Include Area Code): 255-2012 / 22c. OFFICE SYMBOL: AFIT/ENP

DD Form 1473, JUN 86 *Previous editions are obsolete.* SECURITY CLASSIFICATION OF THIS PAGE